Quaternary Research 84 (2015) 398–414

Contents lists available at ScienceDirect

Quaternary Research

journal homepage: www.elsevier.com/locate/yqres

Climatic implications of the Quaternary fluvial tufa record in the NE Iberian Peninsula over the last 500 ka

Carlos Sancho [a,*], Concha Arenas [a], Marta Vázquez-Urbez [a], Gonzalo Pardo [a], María Victoria Lozano [b], José Luis Peña-Monné [c], John Hellstrom [d], José Eugenio Ortiz [e], María Cinta Osácar [a], Luis Auqué [a], Trinidad Torres [e]

[a] Departamento de Ciencias de la Tierra, Universidad de Zaragoza, Pedro Cerbuna 12, 50009 Zaragoza, Spain
[b] Departamento de Geografía y Ordenación del Territorio, Universidad de Zaragoza, Ciudad Escolar s/n, 44003 Teruel, Spain
[c] Departamento de Geografía y Ordenación del Territorio, Universidad de Zaragoza, Pedro Cerbuna 12, 50009 Zaragoza, Spain
[d] School of Earth Sciences, The University of Melbourne, VIC 3010, Melbourne, Australia
[e] Laboratorio de Estratigrafía Biomolecular, Escuela Técnica Superior de Ingenieros de Minas, Ríos Rosas 21, 28003 Madrid, Spain

ARTICLE INFO

Article history:
Received 4 March 2015
Available online 31 October 2015

Keywords:
Fluvial tufas
Dating techniques
Quaternary climate
Iberian Ranges

ABSTRACT

The drainage area of the Iberian Ranges (NE Spain) houses one of the most extensive Quaternary fluvial tufaceous records in Europe. In this study, tufa deposits in the Añamaza, Mesa, Piedra and Ebrón river valleys were mapped, stratigraphically described and chronologically referenced from U/Th disequilibrium series, amino acid racemization and radiocarbon methods. Tufa deposits accumulated in cascades, barrage-cascades and related damming areas developed in stepped fluvial systems. The maximum frequency of tufa deposition was identified at 120 ka (Marine Oxygen Isotope Stage [MIS] 5e), 102 ka (MIS 5c), 85 ka (~MIS 5a) and 7 ka (MIS 1), probably under warmer and wetter conditions than today. Additional phases of tufa deposition appear at ~353 ka (~end of MIS 11), 258–180 ka (MIS 7) and 171–154 ka (MIS 6). Although most tufa deposition episodes are clearly correlated with interstadial periods, the occurrence of tufa deposits during the penultimate glaciation (MIS 6) is remarkable, indicating that the onset of this stage was climatically favourable in the Iberian Peninsula. Biostatic conditions and the dynamics of karstic systems regulating tufa deposition seem to be sensitive to the precipitation regime, controlled by shifts in the position of North Atlantic atmospheric belts, and summer insolation, regulated by orbital forcing.

Introduction

Tufas are terrestrial freshwater deposits of calcium carbonate (Viles and Goudie, 1990) in karstic terrains containing the remains of macro- and microphytes, invertebrates and bacteria (Ford and Pedley, 1996). Tufas can be considered the external sedimentary response to karstic system dynamics. A close relationship between karstic activity, including tufa formation, and environmental conditions is established in terms of suitable temperature, water availability, vegetation, soil development, carbonate dissolution after infiltration and water discharge saturated in calcite (Henning et al., 1983; Magnin et al., 1991; Baker et al, 1993; Martín-Algarra et al., 2003; Brasier, 2011; Domínguez-Villar et al., 2011; Capezzuoli et al., 2014; Della Porta, 2015; among others). Consequently, tufa records are a useful tool to decipher long-term Quaternary climatic changes because they can be accurately placed in time by using several dating techniques.

The palaeoclimate interpretation of tufa archives (Ford and Pedley, 1996; Pedley et al., 1996) seems to indicate that temperature is the limiting factor in temperate areas of high latitude (Frank et al., 2000; Pazdur et al., 1988; Pedley, 1993), while precipitation could limit tufa formation in low-latitude regions (Cremaschi et al., 2010; Kronfeld et al., 1988; Livnat and Kronfeld, 1985; Smith et al., 2004; Viles et al., 2007). In fact, Henning et al. (1983) proposed a different distribution in the age-frequency data of tufa formation under both temperate and Mediterranean environments over the last 350 ka. This simple pattern controlled by precipitation becomes more complex in the Iberian Peninsula due to its high sensitivity to shifts of the North Atlantic atmospheric belts (Cacho et al., 2002; Calvo et al., 2001; Eynaud et al., 2009; Moreno et al., 2005) but also because of the influence of both Atlantic and Mediterranean atmospheric fronts (Pérez-Sanz et al., 2013). In this way, paleoclimate information derived from the fluvial tufa record in the northeastern Iberian Peninsula can significantly contribute to improve the available palaeoenvironmental framework at the Mediterranean scale during the Quaternary.

Tufas are present in a wide range of karst environments around the world and are very common in alpine ranges of the Mediterranean

* Corresponding author.
E-mail address: csancho@unizar.es (C. Sancho).

http://dx.doi.org/10.1016/j.yqres.2015.08.003
0033-5894/

region, reaching relevance in the Iberian Peninsula (Durán, 1989; Ford and Pedley, 1996; Pedley, 2009; Pentecost, 1995). Specifically, the Iberian Ranges (NE Spain) house an exceptional tufa record through time and space that is mainly associated with the low- and medium-order stretches of fluvial network. Although palaeoenvironmental studies of Iberian Range tufas have recently experienced a significant surge (e.g., Domínguez-Villar et al., 2011; Ortiz et al., 2009; Vázquez-Urbez et al., 2011a), these advances can be supplemented with new data. This study contributes to improving the palaeoclimatic information in the northeastern Iberian Peninsula by using a compilation of chronological data from Quaternary fluvial tufa records in the Añamaza, Mesa, Piedra and Ebrón rivers valleys (Fig. 1).

The palaeoenvironmental implications derived from tufaceous archives, supported by a new chronological database by using U/Th series dating, amino acid racemization and radiocarbon dating, has been applied to the Middle–Upper Pleistocene and Holocene regional paleoclimatic context. Thus far, only glacial and fluvial archives have been used to infer cold signatures within a biassed palaeoenvironmental scenario (Benito et al., 2010; Calle et al., 2013; Fuller et al., 1998; García-Ruiz et al., 2013; Lewis et al., 2009). Moreover, the deduced long-term (multi-millennial) climatic changes have been correlated with the Quaternary climate pattern at both Mediterranean and global scales. Preliminary chronological data and paleoclimatic interpretations of local tufa records from the studied sector of the Iberian Ranges have been supplied by Arenas et al. (2010), Sancho et al. (2010) and Lozano et al. (2012).

Studied areas in the Iberian Ranges

The Iberian Ranges are a NW–SE trending alpine intraplate mountain chain located in the north-eastern Iberian Peninsula (Fig. 1). This mountain range is approximately 500 km in length reaching the Mediterranean coast. The highest peaks range between 1813 m (Penyagolosa, SE sector) and 2313 m (Moncayo, NW sector) in altitude.

The landscape is dominated by extensive high-altitude platforms and planation surfaces (1600–1000 m asl) partitioned by tectonic grabens. The formation of the most extensive planation surface (*Superficie de Erosión Fundamental* of the Iberian Ranges) (Peña et al., 1984) was

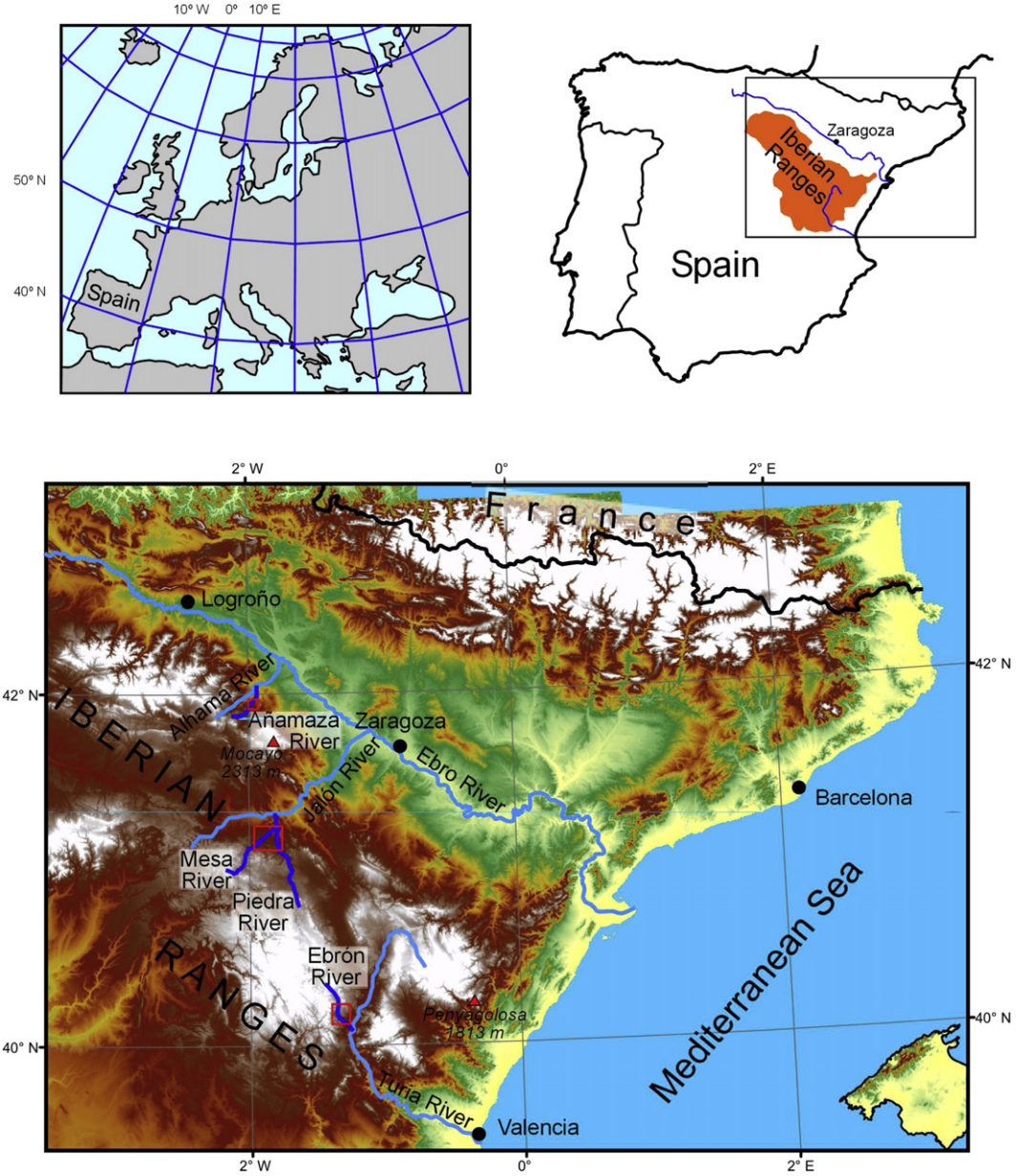

Fig. 1. Location of the studied areas (valleys of the Añamaza, Mesa, Piedra and Ebrón rivers) in the Iberian Ranges (NE Iberian Peninsula).

https://doi.org/10.1016/j.yqres.2015.08.003 Published online by Cambridge University Press

concluded during the Pliocene (Gutiérrez and Peña, 1994). It erodes the alpine compressional structures affecting thick and extensive marine carbonate formations that are Jurassic and Upper Cretaceous in age. An intensive karstic period led to the formation of large fields of dolines and poljes occurred during the final stage of the planation surface development. The resulting erosive surface was partitioned by extensional tectonics during the Pliocene and Quaternary (Gutiérrez and Peña, 1994). This morphotopographic framework constitutes the starting point for the subsequent fluvial downcutting during the Quaternary (Gutiérrez et al., 2008; Scotti et al., 2014).

The formation of tufas in the Iberian Ranges was triggered by the occurrence of high-altitude, extensive limestone flattened areas partitioned by neotectonics and dissected by a fluvial network with non-equilibrium longitudinal stretches, steep gradients and marked

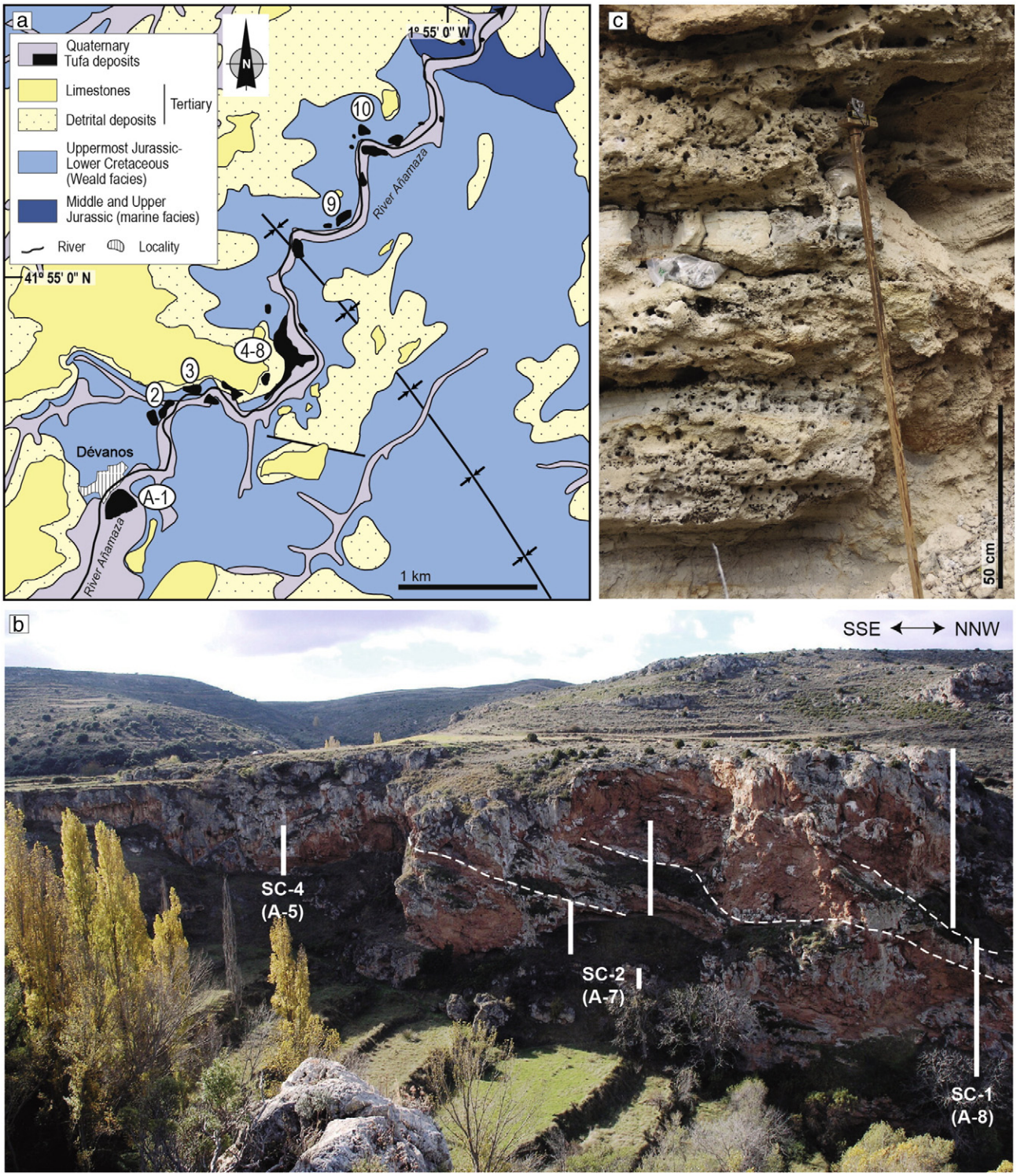

Fig. 2. Añamaza valley area. Dévanos is at 41°54′12″N 1°56′50″W. a) Geological map (modified from Arenas et al., 2014b), with location of stratigraphic sections and other studied sites (A-1 to 10). b) Field view of a wedge-shaped tufa deposit (Salto del Cajo), with indication of the stratigraphic sections (A-5, A-7 and A-8) shown in Fig. 5. c) Detail of section A-10 (2–4 m along the vertical log), consisting of dominant carbonate sand and silt.

https://doi.org/10.1016/j.yqres.2015.08.003 Published online by Cambridge University Press

knick points. Under this morphostructural framework, tufa accumulation was increased during favourable intervals with high discharge of water saturated in calcite from karstic aquifers and warm environmental conditions.

In the Iberian Ranges, the most important tufa build-ups are associated with the drainage network flowing radially to the N and NE (into the Ebro depression), to the SW (into the Tajo and Guadiana depressions) and to the SE (into the Mijares, Turia and Júcar depressions).

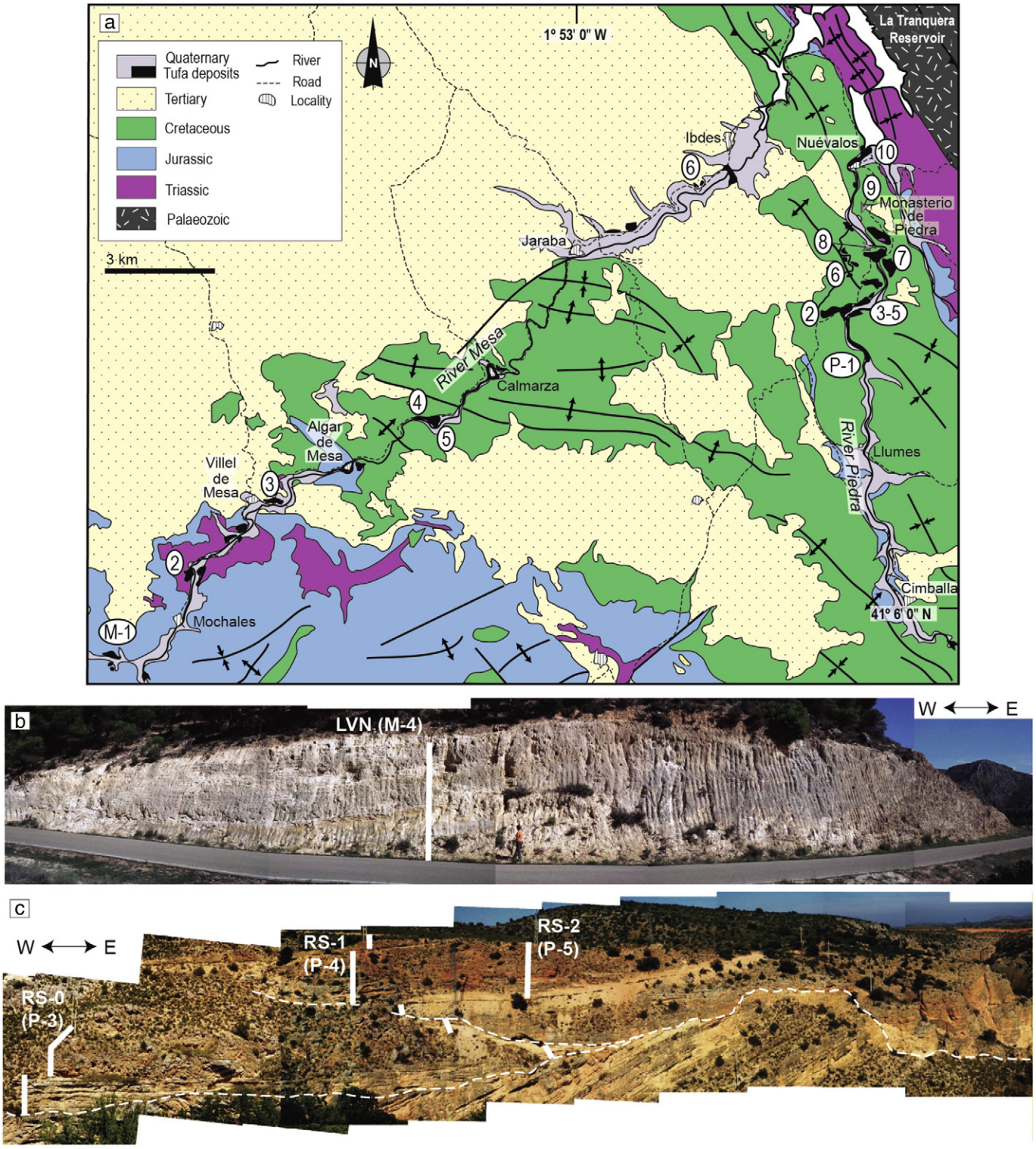

Fig. 3. Mesa and Piedra valley areas. Calmarza is at 41°09′28″N 1°54′42″W. a) Geological map (modified from Vázquez-Urbez et al., 2012), with location of stratigraphic sections and other studied sites (M-1 to 6 and P-1 to 10). b) Field view of tufa deposits (Los Villarejos N; M-4 section) in the Mesa Valley. Thick carbonate sand and silt deposits that grade eastward to moss and hanging-stem boundstones. c) Field view of tufa deposit (La Requijada) in the Piedra valley, with indication of the stratigraphic sections (P-3, P-4 and P-5) shown in Fig. 7. Note the angular unconformity of the Quaternary deposits over Tertiary and Cretaceous rocks.

https://doi.org/10.1016/j.yqres.2015.08.003 Published online by Cambridge University Press

The studied Quaternary fluvial tufa records (Figs. 2, 3 and 4) are located in the valleys of the Añamaza, Mesa and Piedra rivers, tributaries of the Ebro River, and the Ebrón River, a tributary of the Turia River (Fig. 1). Some characteristics of the studied river valleys have been summarized in Table 1.

The current tufa dynamics has been studied by Auqué et al. (2014) in the Añamaza River, Auqué et al. (2013) in the Mesa River, Vázquez-Urbez et al. (2010), Osácar et al. (2013) and Arenas et al. (2014a) in the Piedra River and Arenas et al. (2015) in the Ebrón River.

Materials and methods

Chronological study of Quaternary tufa records requires geological mapping as well as detailed geomorphic and stratigraphic control of the identified tufa build-ups prior to sampling and dating (Figs. 2a, 3a, 4a, 5a, 6a, 7a and 8a). In the first stage, geological mapping of tufa outcrops along the Añamaza, Mesa, Piedra and Ebrón valleys was undertaken using an aerial photographic base (1:18,000 scale). Later, intensive field work was carried out to check the mapped tufa build-ups, to

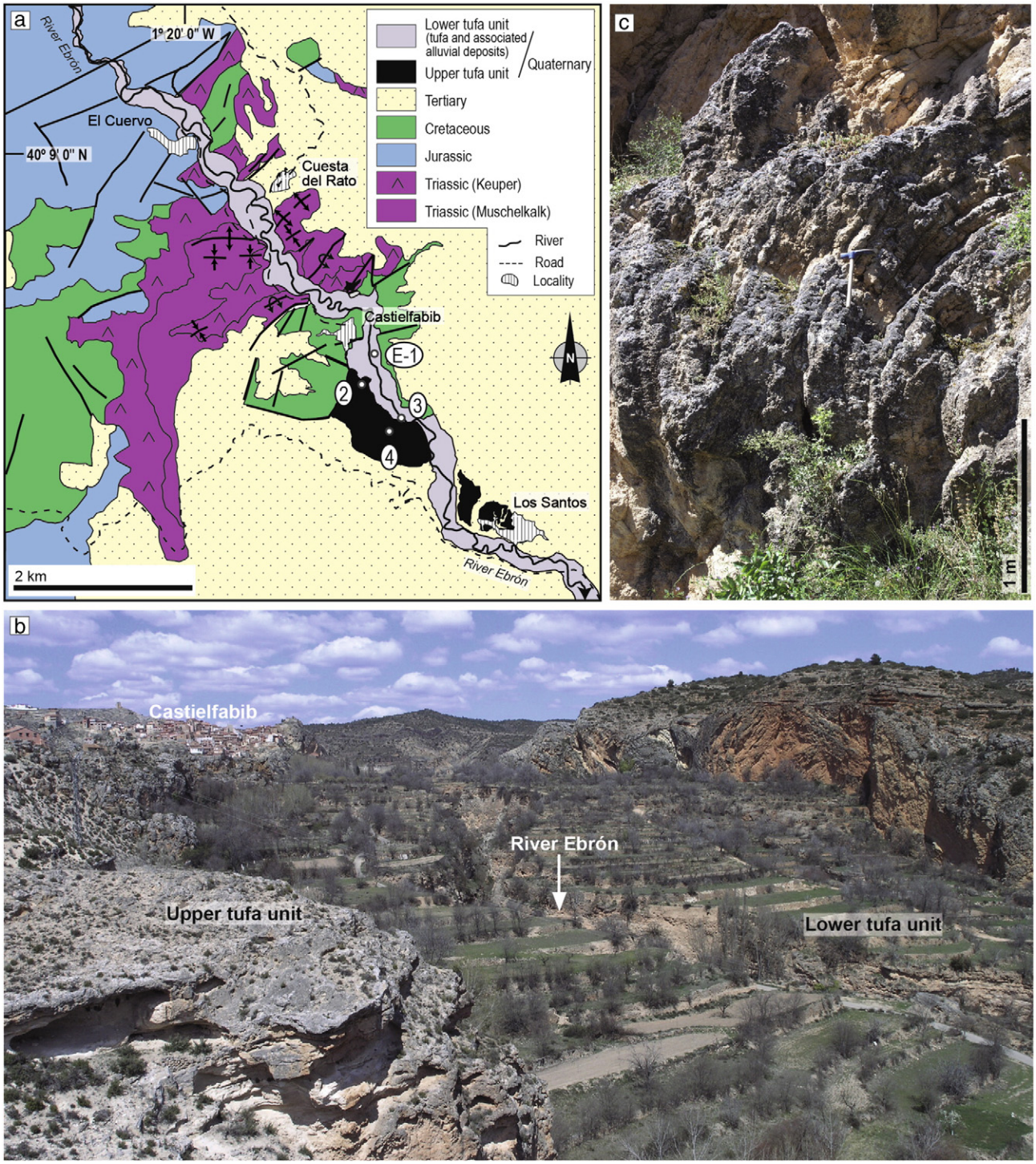

Fig. 4. Ebrón valley area. Castielfabib is at 40°7′50″N 1°18′16″W. a) Geological map (modified from Lozano et al., 2012), with location of stratigraphic sections (E-1 to 4). b) Field view of the valley, showing the two main Quaternary deposition stages arranged in an encased terrace sequence. c) Detail of a moss boundstone from section E-2 (Cascada).

https://doi.org/10.1016/j.yqres.2015.08.003 Published online by Cambridge University Press

Table 1
Summarized information on the studied valleys (location, climate, hydrology and drainage area). Annual discharge from available data in http://www.chebro.es (Añamaza, Mesa and Piedra rivers) and http://www.chj.es (Ebrón River).

River valley	Headwaters coordinate	Altitude range (m)	Annual precipitation (mm/yr)	Mean annual temperature (°C)	Drainage area (km^2)	Channel length (km)	Mean discharge over the year (m^3/s)	Geological bedrock of catchment basin
Añamaza	41°52′30″N 02°06′25″W	1040–460	520	11.2	210	39	0.16	Jurassic limestones and marls Cretaceous sandstones and mudstones Tertiary conglomerates, sandstones and limestones
Mesa	40°57′5″N 02°06′07″W	1520–690	410	13	622	50	1.58	Triassic sandstones, dolostones and gypsum Jurassic and Cretaceous limestones and dolostones Miocene conglomerates, sandstones and mudstones
Piedra	40°55′06″N 01°51′13″W	1010-600	370	13.7	1545	41	1.22	Jurassic limestones Lower Cretaceous sandstones Upper Cretaceous limestones and dolostones Tertiary conglomerates, sandstones and mudstones
Ebrón	40°16′55″N 01°24′22″W	1720–720	450	10.8	246	42	1.20	Triassic dolostones, mudstones and gypsums Jurassic limestones Cretaceous sandstones and dolostones Tertiary conglomerates, sandstones and mudstones

distinguish morphosedimentary units, to describe the selected stratigraphic sections and, finally, to sample for dating. A multi-technique strategy that included U/Th disequilibrium series (U/Th), amino acid racemization (AAR) and radiocarbon (^{14}C) methods was developed according to the tufa facies characteristics and the expected age of the deposits. A total of 93 ages are presented in our study. Because not all of

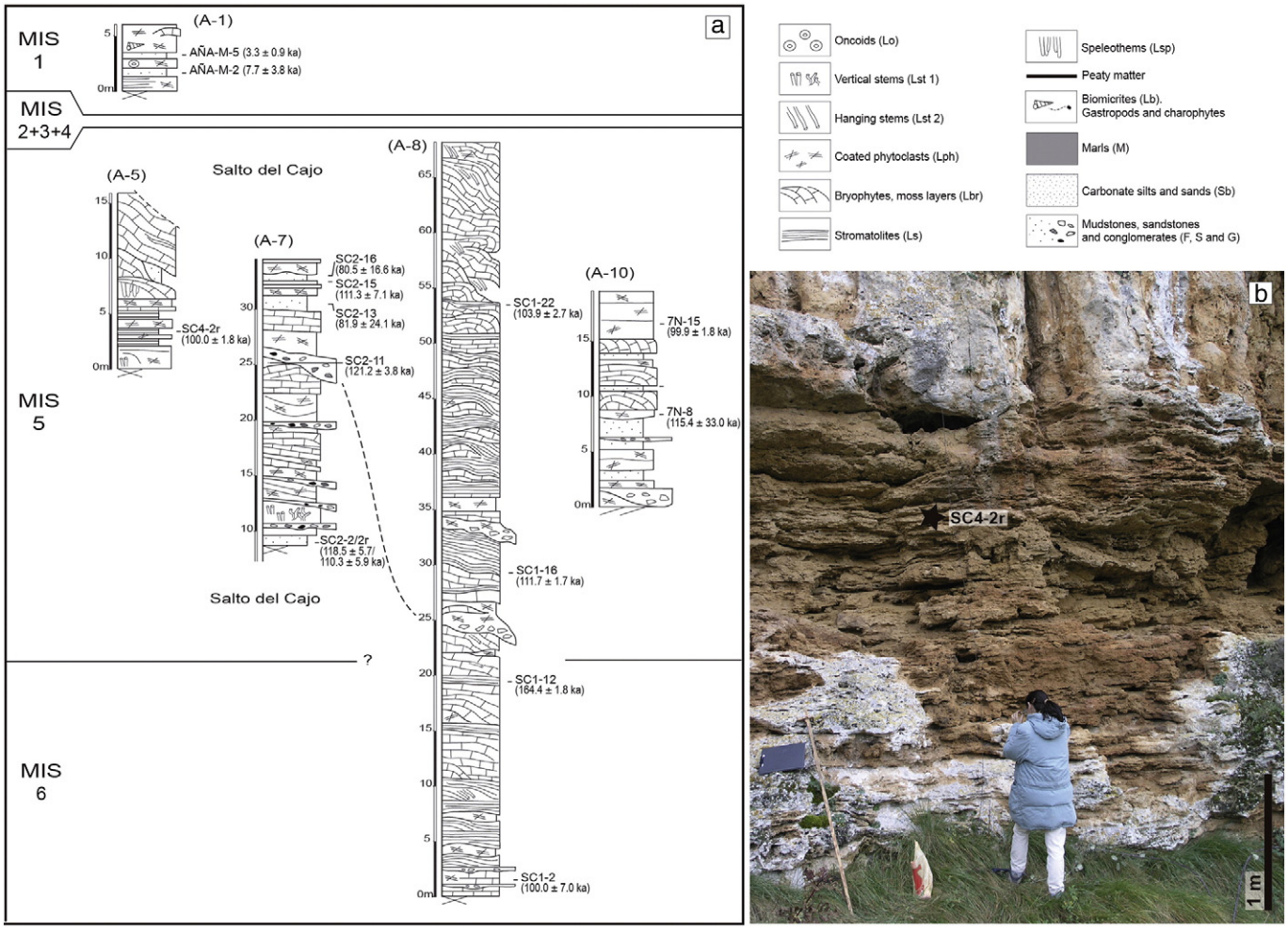

Fig. 5. a) Stratigraphic sections of the Añamaza valley and their correlation (location of sections in Fig. 2). Note the positions of samples used for dating and correspondence to MIS. Only samples that yielded reliable ages are indicated. b) Field view of the lower portion of the stratigraphic section A-5 (Salto del Cajo). Position of a dated sample (black star) is also indicated in the picture.

https://doi.org/10.1016/j.yqres.2015.08.003 Published online by Cambridge University Press

the samples have the same level of reliability and certainty, two techniques were applied simultaneously to the same stratigraphic section when possible. Sometimes replicated ages were obtained. Although discrete ages for individual tufa samples may be subject to selection biases, the set of samples from a particular build-up allows us to define the time elapsed for its accumulation. Consequently, the population of data appears to be representative of the major stages of tufa formation in the Iberian Ranges.

U/Th disequilibrium series

Uranium–thorium disequilibrium dating was performed at the School of Earth Sciences of the University of Melbourne using parallel ion-counting multi-collector ICP-MS (Hellstrom, 2003). A total of 35 samples from tufa build-ups outcropping in the valleys of the four rivers was analysed (Table 2). The samples correspond to various facies: stromatolites, boundstones of bryophytes and of other macrophyte stems, rudstones of oncoids and mudstones to packstones of bioclasts, in all cases avoiding cements. The data quality is variable and depends on the initial amount of detrital Th, the post-depositional locking of the geochemical system and the recrystallization processes. Many samples show contamination with external Th. In these cases, corrected ages for detrital Th were calculated according to Eq. 1 of Hellstrom (2006). In open systems, the post-deposition uranium mobility usually leads to U loss, which makes samples appear older than their real ages (because the Th/U ratio is increased). Tufa is permeable to groundwater and is thus susceptible to the open-system behaviour of uranium, which can be tested for using replicate analyses or other external age constraints. Despite inconveniences observed in the application of U/Th on tufa deposits, the obtained ages contribute to the establishment of a reasonably accurate chronological framework.

Amino acid racemization

A total of 48 samples from tufa build-ups, corresponding to carbonate silts and sands, located in the four fluvial valleys was analysed using AAR methods (Table 3). Ostracode specimens from various species were recovered, although we selected mostly *Herpetocypris reptans* for the analysis because it is the most common in the tufa deposits of the Iberian Peninsula. In some few cases, where *H. reptans* was absent or scarce, *Cyprideis torosa, Candona neglecta*, *Candona marchica* and *Ilyocypris gibba* shells were selected. The species were also subjected to age calculation algorithms (Ortiz et al., 2004). However, because certain genera show different amino acid racemization rates (Ortiz et al., 2013) a conversion factor had to be applied to the D/L ratios of these species to be directly comparable with *H. reptans* aspartic and glutamic D/L values. In general, *H. reptans* valves show slightly higher Asp D/L values than *Candona* and *Ilyocypris* specimens (0.01 to 0.02) in samples with D/L < 0.25, but this difference is larger (0.05 to 0.08) for samples with D/L values ranging from 0.25 to 0.40 (Ortiz et al., 2013). In older samples, the difference in Asp D/L is almost negligible. Glu D/L values were similar in *Candona* and *Herpetocypris* specimens for low D/L values (<0.09). However, in the Glu D/L range between 0.09 and 0.18, *Herpetocypris* valves racemized faster than those belonging to *Candona*. *Ilyocypris* valves showed similar Glu racemization rates than *Candona*, for Holocene, Upper Pleistocene and Late-Middle Pleistocene localities (Glu D/L < 0.18); but for older localities, differences in the racemization rates of this amino acid for *I. gibba* vs. *C. neglecta* and *H. reptans* valves are notable. Ortiz et al. (2013) provided the equations to transform Asp and Glu D/L values of ostracode genera.

When possible, we performed seven analyses of the same sample. Ostracode valves were carefully cleaned sonically in distilled deionized water and rinsed in the same water to remove sediment. To remove

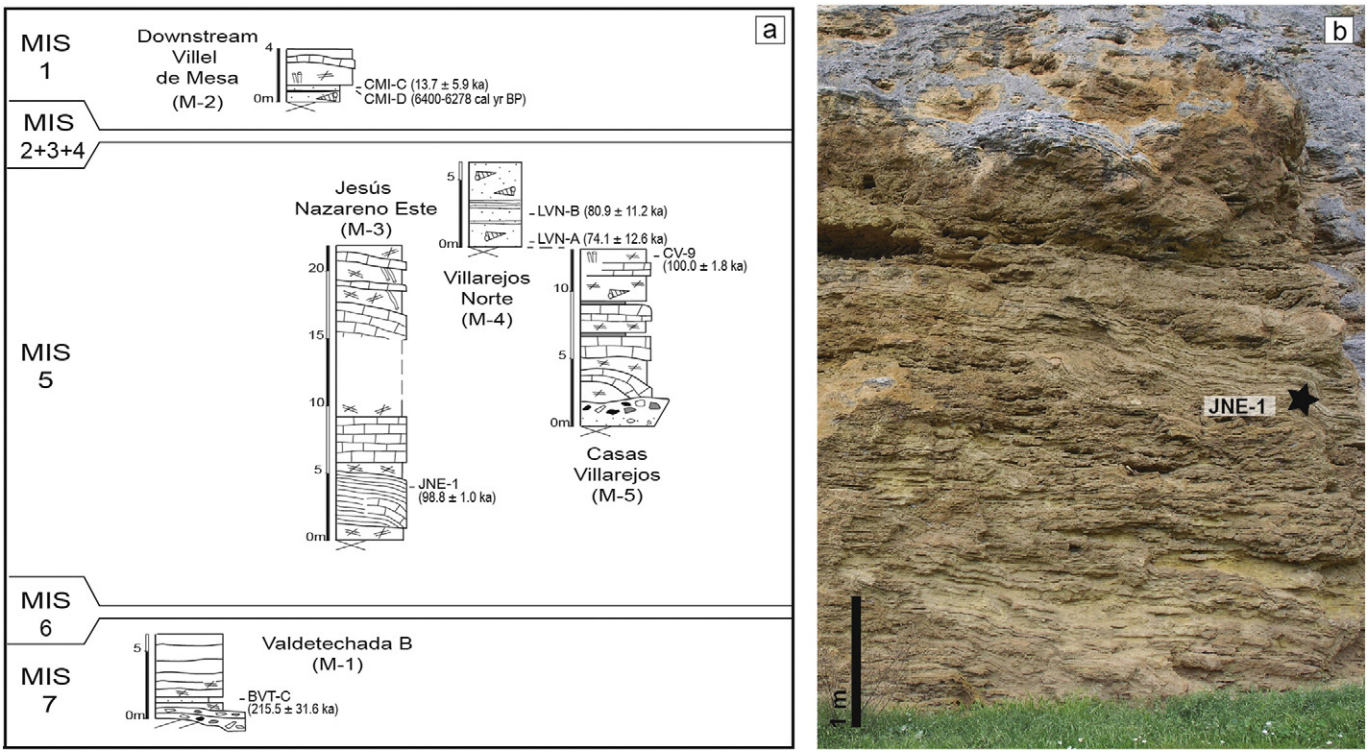

Fig. 6. a) Stratigraphic sections of the Mesa valley and their relative position (location of sections in Fig. 3 and symbol legend in Fig. 5). Note the positions of samples used for dating and correspondence to MIS. Only samples that yielded reliable ages are indicated. b) Field view of the lower part of stratigraphic section M-3 (Jesús Nazareno Este), with abundant stromatolite deposits. Position of a dated sample (black star) is indicated in the picture.

https://doi.org/10.1016/j.yqres.2015.08.003 Published online by Cambridge University Press

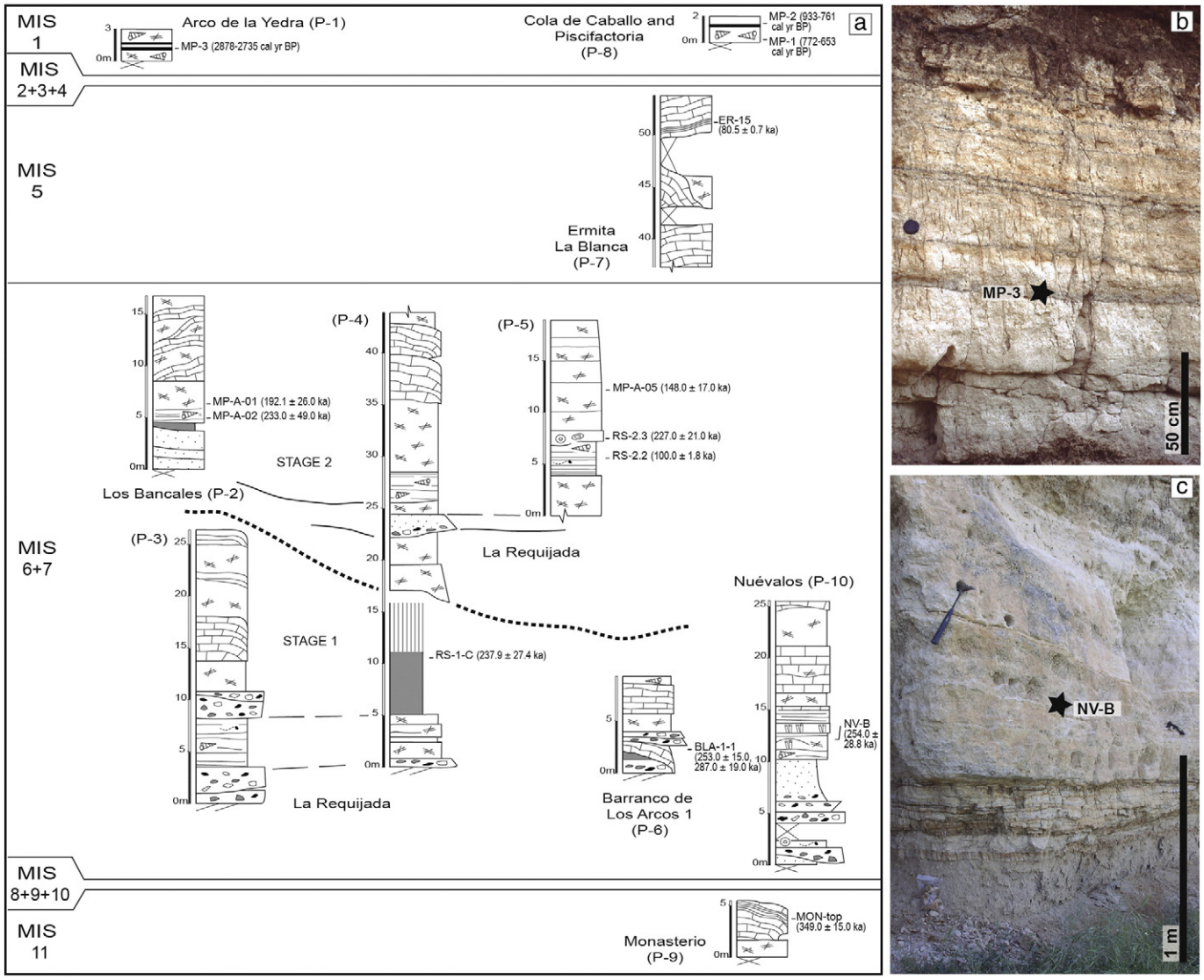

Fig. 7. a) Stratigraphic sections of the Piedra valley and their correlation (location of sections in Fig. 3 and symbol legend in Fig. 5). Note the positions of samples used for dating and correspondence to MIS. Only samples that yielded reliable ages are indicated. b) Field view of stratigraphic section P-1 (Arco de la Yedra). c) Field view of the middle part of stratigraphic section P-10 (Nuévalos). Position of some dated samples (black stars) is also indicated in the pictures.

secondary organic molecules adsorbed to the shells, the valves were then submerged in 3% hydrogen peroxide for 2 h following the methods of Kaufman (2000) and Hearty et al. (2004).

Amino acid concentrations and ratios were quantified using HPLC (high-performance liquid chromatography) at the Biomolecular Stratigraphy Laboratory of the Madrid School of Mines, following the sample preparation protocol described by Kaufman and Manley (1998) and Kaufman (2000).

We measured D/L values of aspartic acid and glutamic acid because in most ostracode valves, they account for over ca. 50% of the amino acid content (Bright and Kaufman, 2011; Kaufman, 2000). Likewise, they have high racemization rates, thus making them suitable for dating relatively young samples. The numerical age of each sample was determined by introducing the aspartic acid and glutamic acid D/L ratios obtained from the ostracodes into the age calculation algorithms established by Ortiz et al. (2004). The age of a sample is the average of the numerical dates. The age uncertainty is one standard deviation of all the numerical ages calculated from the amino acid D/L values of each sample.

The use of the age calculation algorithms obtained from the central and southern Spain ostracodes by Ortiz et al. (2004) for the dating of these deposits is justified because a similar thermal history can be inferred for these areas, being located in the Mediterranean climatic zone of the Iberian Peninsula, with a similar CMAT (current mean annual temperature). Likewise, the age calculation algorithms were established for the ostracode species analysed here (*C. torosa* and *H. reptans*), which show similar racemization rates for high D/L values (D/L > 0.35) (Ortiz et al., 2013), and therefore, the D/L ratios are directly comparable without any conversion factor.

The results of some samples were rejected based on the high concentration of the amino acid L-serine with respect to that of L-aspartic acid, which would indicate contamination of valves by modern amino acids, as serine decomposes rapidly (cf. Kaufman, 2006).

Radiocarbon

Radiocarbon dating was performed on ten samples taken from different tufa build-ups outcropping in the four valleys (Table 4). The

https://doi.org/10.1016/j.yqres.2015.08.003 Published online by Cambridge University Press

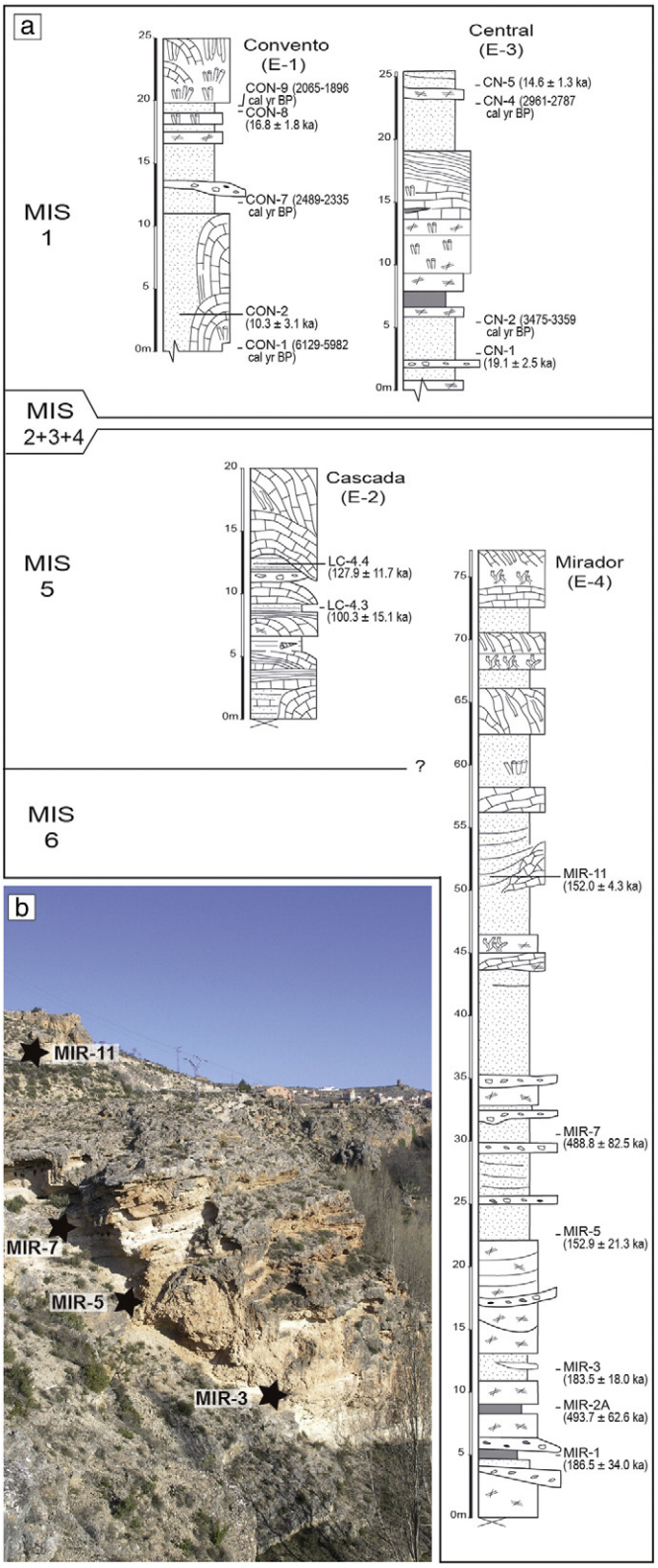

Fig. 8. a) Stratigraphic sections of the Ebrón valley and their relative position (location of sections in Fig. 4 and symbol legend in Fig. 5). Note the positions of samples used for dating and correspondence to MIS. Only samples that yielded reliable ages are indicated. b) Field view of stratigraphic section E-4 (Mirador) (approximately 15 to 65 m). Position of some dated samples (black stars) is also indicated in the picture.

samples correspond to grey peaty intervals and charcoal remnants. Several, gastropods and eggshells were also dated. The dating analyses were carried out in the Radiocarbon Laboratory of the Department of Geography at the University of Zurich. The accelerator mass spectrometer used was the tandem accelerator of the Institute of Particle Physics at the Swiss Federal Institute of Technology Zurich. Radiocarbon ages were calibrated using the Calib6 programme and the IntCal09 calibration curve (Reimer et al., 2009; Stuiver and Reimer, 1993).

Results

General stratigraphic and sedimentological features of fluvial tufas

Fluvial tufa deposits appear as successive build-ups that crop along the main, and some secondary, valleys as stepped terraces in longitudinal profiles as well as transverse sections. In all cases, tufa morphosedimentary units lie unconformably on the bedrock conforming sequences of cut-and-fill and nested-fill terraces. Commonly, these build-ups are composed of lenticular and wedge-shaped bodies that open downstream, with lenticular (channel-like) transverse sections. The thickness of single build-ups ranges from a few metres up to 90 m, and their extent can reach ca. 1.5 km with a width of several hundred metres.

A wide variety of sedimentary facies make up these deposits (Figs. 5a, 6a, 7a and 8a): stromatolites (Ls), bryophyte (Lbr) and other macrophyte stem (up-growing plants, Lst 1; down-growing plants, Lst 2) boundstones, phytoclast (Lph) and oncoid (Lo) rudstones, bioclast and intraclast mudstones to packstones (Lb), marls (M) and carbonate, mainly bioclastic, sands and silts (Sb). The latter two facies may contain variable amounts of microscopic and macroscopic organic matter, in some cases approaching peaty intervals. Gravels, conglomerates (G), sands, sandstones (S) and mudstones (F) are minor components; typically, coarse facies appear related to erosional surfaces.

Facies Ls, Lbr and Lst 2 constitute highly inclined to vertical strata, which, in most cases, make up hemi-domed bodies up to several metres high. Lenticular bodies of phytoclastic facies (Lph) are commonly interbedded. All these facies formed in typically fast-flowing water conditions: cascades, barrage-cascades and moderate-sloped river stretches. In contrast, facies Lb, Sb, Lph, M and minor Ls and Lo mostly compose horizontal and slightly inclined strata. Facies Lb, Sb, Lph, Lo and M formed in slow-flowing and standing-water areas dammed by barrage-cascades. Oncolites can also be structured as shallow, low-sinuosity bars. Stromatolites also developed in moderate-sloped river stretches between cascades. Boundstones consisting of up-growing plants (Lst 1) formed in moderate- to slow-flowing water conditions, both along free-flowing river stretches and standing-water areas (e.g., palustrine conditions) (Arenas-Abad et al., 2010; Vázquez-Urbez et al., 2012). Coarse detrital facies (G, S and Lph) appear related to erosional surfaces at the base of the tufa build-ups, but also within them, giving rise to composite build-ups (i.e., made of several lenticular and wedged bodies) (Arenas et al., 2014b; Vázquez-Urbez et al., 2012).

The geometry of deposits, facies associations and lateral relations among facies within build-ups conform the barrage-cascade model (Pedley, 1990; 2009) or stepped fluvial system (Arenas-Abad et al., 2010), consisting of cascade and barrage-cascade structures laterally related to dammed areas. However, distinct attributes characterize each of the studied fluvial systems, mostly as a function of variations in slope along the valley and as the result of existing diffluence processes. The Añamaza deposits correspond to both moderate and very high-sloped fluvial systems, which respectively determined the presence of large pooled areas (e.g., in the upper part of the valley) and of steep river stretches dominated by facies Ls and Lbr (e.g., in the middle part of the valley) (Arenas et al., 2014b). In the Mesa valley, the moderate slope conditioned the development of large dammed areas, with wide palustrine fringes, separated by barrage-cascades. In contrast, the outstanding feature of the Piedra River tufas is the abundance of thick barrage-cascade deposits in the middle-low stretch as a result of increased slope. At some moments, the height of the barrages surpassed the water divide and caused the upstream dammed areas to spill over

https://doi.org/10.1016/j.yqres.2015.08.003 Published online by Cambridge University Press

Table 2
U/Th disequilibrium series data and ages.

River valley	Section	Sample	Tufa facies	Lab number	U (ngg^{-1})	$[^{230}Th/^{238}U]$[a]	$[^{234}U/^{238}U]$[a]	$[^{232}Th/^{238}U]$	$[^{230}Th/^{232}Th]$	Age (ka)[b]	$[^{234}U/^{238}U]_i$[c]
Añamaza	A-10	ANA 7 N-15	Stromatolitic coating	UMA02818	n.a.	1.4870(47)	2.2823(43)	0.02840(38)	52	99.9 ± 1.8	2.7000(96)
	A-9	ANA 8-1	Stromatolitic coating	UMA02819	n.a.	2.000(24)	1.830(93)	0.006023(96)	332	338.0 ± 110.0	3.17(65)
		ANA 8-5	Oncolite	UMA02820	n.a.	1.668(10)	2.285(10)	0.03315(11)	50	119.4 ± 2.5	2.799(15)
		ANA 9-1r	Phytoclast	UMA03223	483	1.0689(58)	2.285(10)	0.012070(38)	89	–	–
		ANA 9-3r	Bioclastic limestone	UMA03224	209	1.292(15)	1.0892(28)	1.8731(46)	0.69	220.0 ± 880.0	1.178(83)
	A-3	ANA 13-2	Stromatolite	UMA02823	n.a.	1.530(26)	2.260(25)	0.02849(14)	54	106.0 ± 3.9	2.699(29)
	A-4	SC5-1r	Moss phytoherm	UMA03230	375	0.04047(86)	2.7342(49)	0.002865(10)	14	1.45 ± 0.17	2.7413(50)
	A-5	SC 4-2r	Bioclastic limestone	UMA03229	535	1.976(25)	2.0696(42)	0.033297(85)	59	100.0 ± 1.8	2.903(35)
	A-6	SC3-8r	Stromatolite	UMA03227	608	1.6287(65)	2.2855(44)	0.007315(25)	223	116.3 ± 1.0	2.7846(59)
		SC 3-2r	Bioclastic limestone	UMA03226	330	1.671(10)	2.2297(52)	0.31829(85)	5	105.0 ± 24.0	2.66(11)
	A-7	SC 2-15	Bioclastic limestone	UMA02830	n.a.	1.6140(76)	2.251(10)	0.10789(39)	15	111.3 ± 7.1	2.712(35)
		SC 2-11	Bioclastic limestone	UMA02829	n.a.	1.596(19)	2.176(25)	0.02811(18)	57	121.2 ± 3.8	2.655(27)
		SC2-2r	Bioclastic limestone	UMA03225	327	1.638(12)	2.3074(48)	0.09333(33)	18	110.3 ± 5.9	2.785(30)
		SC 2-2	Bioclastic limestone	UMA02828	n.a.	1.627(17)	2.209(17)	0.07927(40)	21	118.5 ± 5.7	2.689(30)
	A-8	SC 1-22	Stromatolite	UMA02827	n.a.	1.515(17)	2.279(26)	0.014844(95)	102	103.9 ± 2.7	2.715(27)
		SC 1-16	Stromatolite	UMA02826	n.a.	1.590(12)	2.288(12)	0.007794(46)	204	111.7 ± 1.7	2.766(13)
		SC 1-12	Stromatolite	UMA02825	n.a.	1.631(11)	1.9061(93)	0.012784(38)	128	164.4 ± 1.8	2.441(12)
		SC 1-2	Phytoclast	UMA02824	n.a.	1.991(12)	1.8809(47)	0.02747(13)	72	100.0 ± 7.0	2.960(36)
Mesa	M-5	CV 9-1	Bioclastic limestone	UMA00996	n.a.	1.0320(43)	1.8268(49)	0.05340(32)	19	100.0 ± 1.8	2.036(14)
		CV 9-2	Bioclastic limestone	UMA00997	n.a.	1.0298(42)	1.8072(40)	0.06944(54)	15	100.0 ± 1.8	2.010(18)
	M-3	JNE 1-1	Stromatolite	UMA00998	n.a.	1.1802(39)	1.8588(49)	0.009823(54)	120	98.8 ± 1.0	2.1351(59)
Piedra	P-6	BLA 1-1.1	Stromatolite	UMA00886	295	1.643(14)	1.6207(33)	0.1624(83)	10	253.0 ± 15.0	2.267(55)
		BLA 1-1.2	Stromatolite	UMA00887	358	1.7346(90)	1.6463(46)	0.2206(10)	8	287 ± 19.0	2.452(75)
	P-7	ER 15	Stromatolite	UMA00888	414	1.1916(63)	2.1514(49)	0.00527(15)	226	80.5 ± 0.7	2.4452(58)
	P-9	MON Top	Stromatolite	UMA00889	343	1.496(10)	1.4156(42)	0.0345(25)	43	349.0 ± 15.0	2.112(44)
	P-4	RS 1-3.1	Phytoclast	UMA00890	642	1.8056(89)	1.5373(51)	0.02669(12)	68	–	–
		RS 1-3.2	Phytoclast	UMA00891	488	1.9212(95)	1.5651(45)	0.04101(15)	47	–	–
	P-5	RS 2-2b	Mudstone	UMA00892	269	1.6575(54)	1.7876(48)	0.1264(34)	13	100.0 ± 1.8	2.349(37)
		RS 2-3	Oncolite	UMA00893	354	1.8131(96)	1.8050(62)	0.2629(17)	7	227 ± 21	2.528(90)
Ebrón	E-4	MIR B5-A	Stromatolite	UMA04101	369	1.2205(65)	1.9298(42)	0.00580(18)	211	98.2 ± 1.0	2.2269(54)
		MIR B5-B	Stromatolite	UMA04102	376	1.2366(53)	1.9260(38)	0.00682(15)	181	100.4 ± 0.9	2.2295(49)
		MIR B6-A	Stromatolite	UMA04103	344	1.2340(42)	1.9284(46)	0.001792(36)	688	100.3 ± 0.6	2.2321(51)
		MIR B6-B	Stromatolite	UMA04104	291	1.1390(41)	1.7856(36)	0.004587(86)	248	100.3 ± 0.7	2.0427(43)
	E-2	LC 3-A	Stromatolitic coating	UMA04105	384	1.2637(41)	1.7956(32)	0.000967(20)	1306	117.4 ± 0.7	2.1082(38)
		LC 3-B	Stromatolitic coating	UMA04106	404	1.2685(43)	1.8034(41)	0.000700(13)	1811	117.3 ± 0.8	2.1186(47)

2 − σ uncertainties in brackets are of the last two significant figures presented except for age which is absolute.
[a] Activity ratios determined after Hellstrom (2003) using the decay constants of Cheng et al (2013).
[b] Age in ka before present corrected for intial ^{230}Th using Eq. 1 of Hellstrom (2006) and $[^{230}Th/^{232}Th]_i$ of 1.5 ± 1.5.
[c] Initial $[^{234}U/^{238}U]$ calculated using corrected age.

a secondary course (fluvial diffluence mechanism), which also recorded tufa deposits (Vázquez-Urbez et al., 2011b, 2012). In the Ebrón valley, with moderate to high slope, thick deposits of facies Sb formed in dammed areas upstream of barrage-cascades. In addition, extensive development of stromatolites occurred in some gently sloped stretches between barrages (Lozano et al., 2012).

Tufas of the Añamaza River valley

Tufa deposits crop out along the middle stretch of the Añamaza valley (northeast of Dévanos) (Fig. 2a). Quaternary tufa build-ups are distributed in two main morphosedimentary units forming a staircase terrace system. The thickness is variable, reaching 70 m in the Salto del Cajo build-up (Fig. 2b). Some selected build-ups were sampled for dating (A-1, A-2, A-3, A-4, A-5, A-6, A-7, A-8, A-9 and A-10) (Fig. 2a).

The oldest deposits correspond to site A-9 (Fig. 2a), with an age of 338 ± 110 ka (U/Th sample ANA8-1) (Table 2), although the uncertainty is large.

The Salto del Cajo build-up (Fig. 2b) (A-5, 7 and 8 sections; Figs. 5a and b) is a wedge-shaped body that opens northwards. It is made of five depositional bodies separated by erosional surfaces composing a complex filling of a steep stretch along the longitudinal profile of the river (Arenas et al., 2014b). A broad agreement between chronological data (U/Th and AAR) (Tables 2 and 3) and the stratigraphic correlation among sections was observed. Thus, the depositional stages are dated between 164.4 ± 1.8 (U/Th sample SC1-12; A-8 section) and 80.5 ± 16.6 ka (AAR sample SC2-16). In addition, a cascade tufa unit that overlies previous Pleistocene deposits in the Salto del Cajo yielded an age of 1.45 ± 0.17 ka (A-4 site; U/Th sample SC5-1r).

In the Las Parideras sector (A-3 section) (Fig. 2a), a wedge-shaped tufa build-up that is ca. 17 m thick has been dated. The estimated age of this outcrop could be between 83.5 ± 18.9 (AAR sample AÑA13-1) and 106 ± 3.9 ka (U/Th sample AÑA 13-2). Two other build-ups (A-10 and A-9) (Fig. 5a) located in the northern part of the studied Añamaza valley stretch provide ages of 115.4 ± 33.0 (AAR sample AÑA 7 N-8) to 99.9 ± 1.8 ka (U/Th sample AÑA 7 N-15) for the A-10 section and 129.1 ± 16.8 (AAR sample AÑA 8-4), 121.7 ± 27.0 (AAR sample AÑA 8-3) and 119.4 ± 2.5 ka (U/Th sample AÑA 8-5) for the A-9 section.

Other tufa build-ups encased in Pleistocene tufas are those of El Molino (A-2 section) (Fig. 5a) and Dévanos (A-1 section) (Fig. 2a). Several samples yielded AAR ages of 10.6 ± 3.3 and 10.5 ± 4.4 ka, in Dévanos, and between 7.7 ± 3.8 and 3.3 ± 0.9 ka in El Molino (Table 3). Moreover, an age of 1816–1509 cal yr BP (sample AÑA-M-H) has been obtained by radiocarbon in El Molino (Table 4). Correlative fluviolacustrine sediments studied by Luzón et al. (2011) from drilling cores in the upper stretch of the valley span from 10.6 to 0.6 ka.

In summary, according to the obtained ages, several episodes of tufa deposition correlated to Marine Oxygen Isotope Stages (MIS) 9a, MIS 6, MIS 5 and MIS 1 can be inferred. Most tufas in the Añamaza River valley formed during MIS 5 (130–80 ka) (Figs. 5a and 9a).

Tufas of the Mesa River valley

Tufa build-ups crop out and are scattered along 30 km in the Mesa River valley from the Mochales to Ibdes villages (Fig. 3a). The thickness

https://doi.org/10.1016/j.yqres.2015.08.003 Published online by Cambridge University Press

Table 3
Aspartic acid and glutamic acid D/L values and ages. Tufa facies samples are always carbonate sands and silts.

River valley	Section	Sample	Specie	Analysis	D/L Asp	D/L Glu	Age (ka)
Añamaza	A–1	AÑA–M–2	*H. reptans*	6	0.174 ± 0.008	0.043 ± 0.003	7.7 ± 3.8
		AÑA–M–5	*H. reptans*	7	0.140 ± 0.005	0.041 ± 0.001	3.3 ± 0.9
	A–2	DEB–1	*H. reptans*	7	0.180 ± 0.008	0.050 ± 0.001	10.6 ± 3.3
		DEB–2	*H. reptans*	7	0.186 ± 0.005	0.048 ± 0.004	10.5 ± 4.4
	A–3	AÑA13–1	*H. reptans*	7	0.301 ± 0.006	0.106 ± 0.016	83.5 ± 18.9
	A–10	AÑA7N–3	*C. neglecta*	7	0.353 ± 0.011	0.131 ± 0.006	129.9 ± 11.1
		AÑA7N–8	*H. reptans*	7	0.348 ± 0.030	0.122 ± 0.025	115.4 ± 33.0
		AÑA7N–10	*H. reptans, C. neglecta*	2	0.222 ± 0.011	0.063 ± 0.002	23.2 ± 5.3
	A–9	AÑA8–2	*C. marchica*	1	0.074	0.036	0.8 ± 0.3
		AÑA8–3	*H. reptans*	7	0.338 ± 0.025	0.128 ± 0.017	121.7 ± 27.0
		AÑA8–4	*H. reptans*	1	0.345	0.129	129.4 ± 16.8
	A–7	SC2–13	*H. reptans*	7	0.314 ± 0.021	0.100 ± 0.014	81.9 ± 24.1
		SC2–16	*H. reptans*	7	0.308 ± 0.016	0.101 ± 0.010	80.5 ± 16.6
Mesa	M–6	LR–A	*I. gibba*	3	0.346	0.136 ± 0.023	129.1 ± 20.2
		LR–B	*I. gibba*	7	0.291 ± 0.023	0.115± 0.007	102.8 ± 21.7
	M–4	LVN–A	*H. reptans*	7	0.309± 0.014	0.094 ± 0.003	74.1 ± 12.6
		LVN–B	*H. reptans, C. marchica*	7	0.308 ± 0.015	0.094 ± 0.006	80.9 ± 11.2
	M–1	BVT–A	*H. reptans*	7	0.322 ± 0.015	0.130 ± 0.013	110.4 ± 22.4
		BVT–C	*H. reptans*	5	0.422 ± 0.026	0.212 ± 0.022	215.5 ± 31.6
		BVT–D	*H. reptans*	7	0.403 ± 0.008	0.149 ± 0.006	194.5 ± 24.1
	M–2	CMI–A	*H. reptans, C. machica C. marchica*	2	0.258 ± 0.014	0.065 ± 0.001	46.8 ± 8.2
		CMI–B	*H. reptans*	7	0.158 ± 0.008	0.045 ± 0.006	6.7 ± 2.3
		CMI–C	*H. reptans*	7	0.194 ± 0.012	0.048 ± 0.006	13.7 ± 5.9
	–	RM–1A	*H. reptans*	7	0.166 ± 0.005	0.042 ± 0.002	8.4 ± 2.0
Piedra	P–4	RS–1–A	*H. reptans*	4	0.425 ± 0.022	0.176 ± 0.020	194.5 ± 27.8
		RS–1–B	*C. marchica*	4	0.350 ± 0.019	0.148 ± 0.027	143.2 ± 28.8
		RS–1–C	*H. reptans*	8	0.438 ± 0.019	0.197 ± 0.068	237.9 ± 27.4
	P–10	NV–A	*I. gibba*	2	0.235 ± 0.034	0.099 ± 0.013	65.2 ± 24.9
		NV–B	*H. reptans*	7	0.472 ± 0.023	0.206 ± 0.029	254.0 ± 28.8
	–	NG–A	*H. reptans*	2	0.324	0.131	130.9 ± 29.0
	P–2	MPA–01	*H. reptans, I. gibba*	5	0.404 ± 0.021	0.195 ± 0.016	192.1 ± 26.0
		MPA–02	*H. reptans, I. gibba*	6	0.426 ± 0.043	0.236 ± 0.029	233 ± 49
	P–5	MPA–05	*H. reptans*	1	0.390	0.140	148 ± 17
Ebrón	E–1	CON–2	*H. reptans, C. neglecta, I.gibba*	5	0.173 ± 0.011	0.049 ± 0.001	10.3 ± 3.1
		CON–8	*H. reptans*	5	0.189 ± 0.005	0.064 ± 0.001	16.8 ± 1.8
	E–3	CN–1	*H. reptans*	7	0.199 ± 0.008	0.063 ± 0.002	19.1 ± 2.5
		CN–5	*H. reptans*	2	0.181 ± 0.005	0.061 ± 0.002	14.6 ± 1.3
	E–2	LC–A	*H. reptans*	7	0.376 ± 0.029	0.164 ± 0.016	150.5 ± 25.7
		LC–B	*C. neglecta*	7	0.394 ± 0.020	0.122 ± 0.003	149.9 ± 18.3
		LC–4.3	*H. reptans, C. neglecta*	7	0.338 ± 0.013	0.107 ± 0.008	100.3 ± 15.1
		LC–4.4	*C. neglecta*	7	0.365 ± 0.010)	0.012 ± 0.024	127.9 ± 11.7
	E–4	MIR–1	*H. reptans*	7	0.407 ± 0.038	0.168 ± 0.033	186.5 ± 34.0
		MIR–2A	*C. torosa*	7	0.614 ± 0.022	0.353 ± 0.041	493.7 ± 62.6
		MIR–3	*H. reptans*	7	0.413 ± 0.009	0.174 ± 0.018	183.5 ± 18.0
		MIR–5	*H. reptans, C. neglecta*	7	0.380 ± 0.027	0.142 ± 0.014	152.9 ± 21.3
		MIR–7	*C. neglecta, C. torosa*	7	0.608 ± 0.033	0.350 ± 0.022	488.8 ± 82.5
		MIR–8	*C. neglecta*	7	0.359 ± 0.003	0.112 ± 0.003	114.2 ± 12.5
		MIR–11	*H. reptans*	7	0.384 ± 0.001	0.152 ± 0.006	152.0 ± 4.3

Samples in grey with recent amino acid contamination.

of single build-ups ranges from a few meters to 25 m. The build-ups can be grouped into two generations developing staircase terraces. Several build-ups belonging to the older stage have been chronologically characterized (Valdetechada, M-1 section; Jesús Nazareno, M-3 section; Los Villarejos, M-4 and M-5 sections; and La Rinconada, M-6 section). Two other younger build-ups have also been dated near Villel de Mesa village (M-2 section; Fig. 6a).

The Valdetechada build-up (M-1 section) (Fig. 6a), located upstream of Mochales, is 15–20 m thick. Two samples were dated by AAR (Table 3), yielding ages of 215.5 ± 31.6 (sample BVT-C) and 194.5 ± 24.1 ka (sample BVT-D). In the Los Villarejos Norte outcrop (M-4 section) (Figs. 3b and 6a), the AAR ages obtained for two laterally related samples (LVN-A and LVN-B), located at the top of the build-up, are 74.1 ± 12.6 and 80.9 ± 11.2 ka, respectively. These ages are consistent with two ages obtained by U/Th in the Casas Villarejos profile (M-5 section) (Fig. 6a) (samples CV9-1 and CV9-2). Both samples supplied the same age (100 ± 1.8 ka) (Table 2). In addition, another sample (JNE1.1) (Table 2) from the Jesús Nazareno stratigraphic section (M-3 section) (Figs. 6a and b) gave an age of 98.8 ± 1 ka.

The younger stage of tufa development has been studied in two outcrops located upstream and downstream of Villel de Mesa village (Fig. 3) and has been dated by AAR. Upstream of Villel de Mesa, the dated outcrop has an age of 8.4 ± 2 ka (sample RM1-A, Table 3). In the outcrop downstream of Villel de Mesa (M-2 section) (Fig. 6a), the obtained ages are 46.8 ± 8.2 (sample CMI-A), 6.7 ± 2.3 (sample CMI-

https://doi.org/10.1016/j.yqres.2015.08.003 Published online by Cambridge University Press

Table 4
Radiocarbon data and ages.

River valley	Section	Sample	Tufa facies	Laboratory code	Age yr BP	Cal Age yr BP 2σ
Añamaza	A-1	AÑA-M-H	Eggshells	UZ-5688/ETH-37066	1710 ± 70	1816-1509
Mesa	M-2	CMI-D	Peat	UZ-5862/ETH-40985	5520 ± 35	6400-6278
Piedra	P-8	MP-1	Charcoal	UZ-5194/ETH-30262	760 ± 45	772-653
		MP-2	Gastropods	UZ-5195/ETH-30263	945 ± 45	933-761
	P-1	MP-3	Peat	UZ-5196/ETH-30264	2680 ± 50	2878-2735
Ebrón	E-1	CON-9	Charcoal	UZ-5948/ETH-42057	2030 ± 35	2065-1896
		CON-7	Charcoal	UZ-5947/ETH-42056	2370 ± 35	2489-2335
		CON-1	Charcoal	UZ-5946/ETH-42055	5275 ± 35	6129-5982
	E-3	CN-4	Charcoal	UZ-5950/ETH-42059	2785 ± 35	2961-2787
		CN-2	Charcoal	UZ-5949/ETH-42058	3195 ± 35	3475-3359

B) and 13.7 ± 5.9 ka (sample CMI-C) (Table 3). Another sample (CMI-D), stratigraphically equivalent to CMI-A has a calibrated ^{14}C age of 6400–6278 cal yr BP (Table 4). Thus, the AAR results indicate that this technique does not offer precise ages for Holocene samples.

Briefly, considering the proposed ages for the studied tufa build-ups in the Mesa River valley, several stages of tufa development could be differentiated (Figs. 6a and 9b). The oldest phase (215–194 ka) correlates to MIS 7. The more important stage (130–75 ka) coincides with the MIS 5. It may be that the end of the MIS 6 is also recorded in this tufa deposition period. The occurrence of MIS 3 has been locally determined. Finally, the youngest phase is Early–Middle Holocene in age (6–7 ka) (MIS 1).

Tufas of the Piedra River valley

Fluvial tufa deposits are very extensive and thick in the lower stretch of the Piedra River valley. They are basically located in two sectors: near the Monasterio de Piedra Natural Park and around Nuévalos village (Fig. 3a). Several episodes of tufa formation arranged in cut-and-fill and nested-fill terrace patterns were distinguished.

Several tufa build-ups were studied and sampled (Fig. 7a). According to geomorphic and stratigraphic criteria, they were grouped into an older period (La Requijada, separate P-3, P-4, P-5 sections; Barranco de Los Arcos, P-6 section; Los Bancales, P-2 section; Ermita de la Blanca, P-7 section; Monasterio, P-9 section; and Nuévalos Viejo, P-10 section) and a younger period (Arco de la Yedra, P-1 section; Cola de Caballo and Piscifactoría, P-8 sections).

Several tufa build-ups were studied near the Monasterio de Piedra, which is related to both the Piedra River and the tributary network. The U/Th age obtained for the Monasterio build-up (P-9 section) (Fig. 7a) is 349 ± 15 ka (sample MON Top) (Table 2). In the La Requijada tufa build-up (P-3, P-4 and P-5 sections) (Figs. 3c and 7a), which is some 75 m thick, two main overlapped stages of tufa aggradation separated by an important erosional surface were recognized. Deposits corresponding to the older stage were dated by AAR (sample RS-1-C), and an age of 237.9 ± 27.4 ka was obtained (Table 3). Tufas of the younger stage were also dated, and a U/Th age of 100 ± 1.8 ka was yielded by sample RS-2.2b (Table 2). The Barranco de los Arcos deposits (P-6 section) crop out as several isolated build-ups (Fig. 7a) that reach 20 m in thickness. Two replicated U/Th analyses of a sample, BLA-1.1 and BLA-1.2, have provided ages of 253 ± 15 and 287 ± 19 ka, respectively (Table 2). These deposits were thus correlated with the lower section of the La Requijada build-up. This result, along with the mapping data, allows a fluvial diffluence episode to be determined (Vázquez-Urbez et al., 2011b). The Los Bancales build-up (P-2 section) is an 18–20-m-thick deposit. The three ages obtained by AAR are 233 ± 49 (sample MP-A-02), 192.0 ± 26 (sample MP-A-01) and 148 ± 17 ka (sample MP-A-05) (Table 3). Taking into account these ages, the mapping data and the spatial relationships between tufa deposits, it is possible to argue that the Los Bancales tufa deposit and the upper section of the La Requijada build-up are genetically related. The Los Bancales deposit represents other fluvial diffluence episode in this area (Vázquez-Urbez et al., 2011b). Finally, downstream of La Requijada, the Ermita de la Blanca build-up (P-7 section) (Fig. 7a) is some 70–80 m thick. The top of this deposit (sample ER-15) yielded an U/Th age of 80.5 ± 0.7 ka (Table 2).

Other important tufa deposits have been identified 2–3 km downstream the Monasterio de Piedra, around Nuévalos village (Fig. 3a). In fact, the old village is settled on a ~25-m-thick tufa build-up (P-10 section; Fig. 7a). The lower part of this build-up (Nuévalos Viejo section; P-10 section; Figs. 7a and c) is dated to 254.0 ± 28.8 ka (sample NV-B) according AAR analysis (Table 3).

In addition to the Pleistocene tufa build-ups, several Holocene build-ups, dated by ^{14}C ages, have been recognized along the Piedra River valley (Table 4). In the Arco de la Yedra outcrop (P-1 section) (Figs. 7a and b), sample MP-3, from a peaty level, provided a calibrated age of 2878–2735 cal yr BP. Gastropod shells embedded in moss boundstones (sample MP-2) from the Cola de Caballo (P-8 section) (Fig. 7a) deposit provided an age of 933–761 cal yr BP. Downstream in the valley of the Monasterio de Piedra, the tufa (Piscifactoría; Fig. 7a) deposits have an age of 772–653 cal yr BP (charcoal sample MP-1).

In brief, according to the distribution of the reliable obtained ages, the tufa deposits in the Piedra River correspond to several periods: MIS 11 (350 ka); MIS 7-6, which shows two important pulses (255–230 and 145–195 ka) separated by an important erosional event; MIS 5 (80 ka); and, finally, MIS 1 (2.7–0.8 ka) (Figs. 7a and 9c).

Tufas of the Ebrón river valley

In the valley of the Ebrón River, around Castielfabib village, mapping and field work have allowed the differentiation of tufa deposits corresponding to two encased terraces (Figs. 4a and b). There is a noticeable knick point in the longitudinal profile of the Ebrón River near Castielfabib. Several tufa build-ups were sampled (Fig. 8): the Mirador (E-4 section) and Cascada (E-2 section) stratigraphic sections in the upper-older unit and the Convento (E-1 section) and Central (E-3 section) stratigraphic sections in the lower-younger unit.

The Mirador stratigraphic section (M-4 section) is approximately 77 m thick (Figs. 8a and b). Seven samples were dated by AAR (Table 3). The age (152.9 ± 21.3 ka) of sample MIR-5 has been corrected because the racemization rate of the *Candona* genus is slower than that of the *Herpetocypris* genus. Samples MIR-2A and MIR-7 showed a similar age (~490 ka) (MIS 13), older than the whole set of samples. These samples contained *C. torosa*, indicating waters high in sulphate and chlorine content with a wide range of water salinities. This means that the sampled tufa deposits were likely inherited from older tufa deposits located upstream and fed by water running across the Upper Triassic evaporites. In addition, two samples from the upper part of the stratigraphic section were dated using U/Th (Table 2). The replicated analyses indicate consistent and reliable ages ranging between 98.2 and 100.4 ka (samples MIR B5 and MIR B6). Summarizing, the more reasonable ages point to 186 ka at the bottom, 152 ka in the intermediate stretch and 100 ka in the top of the stratigraphic section.

https://doi.org/10.1016/j.yqres.2015.08.003 Published online by Cambridge University Press

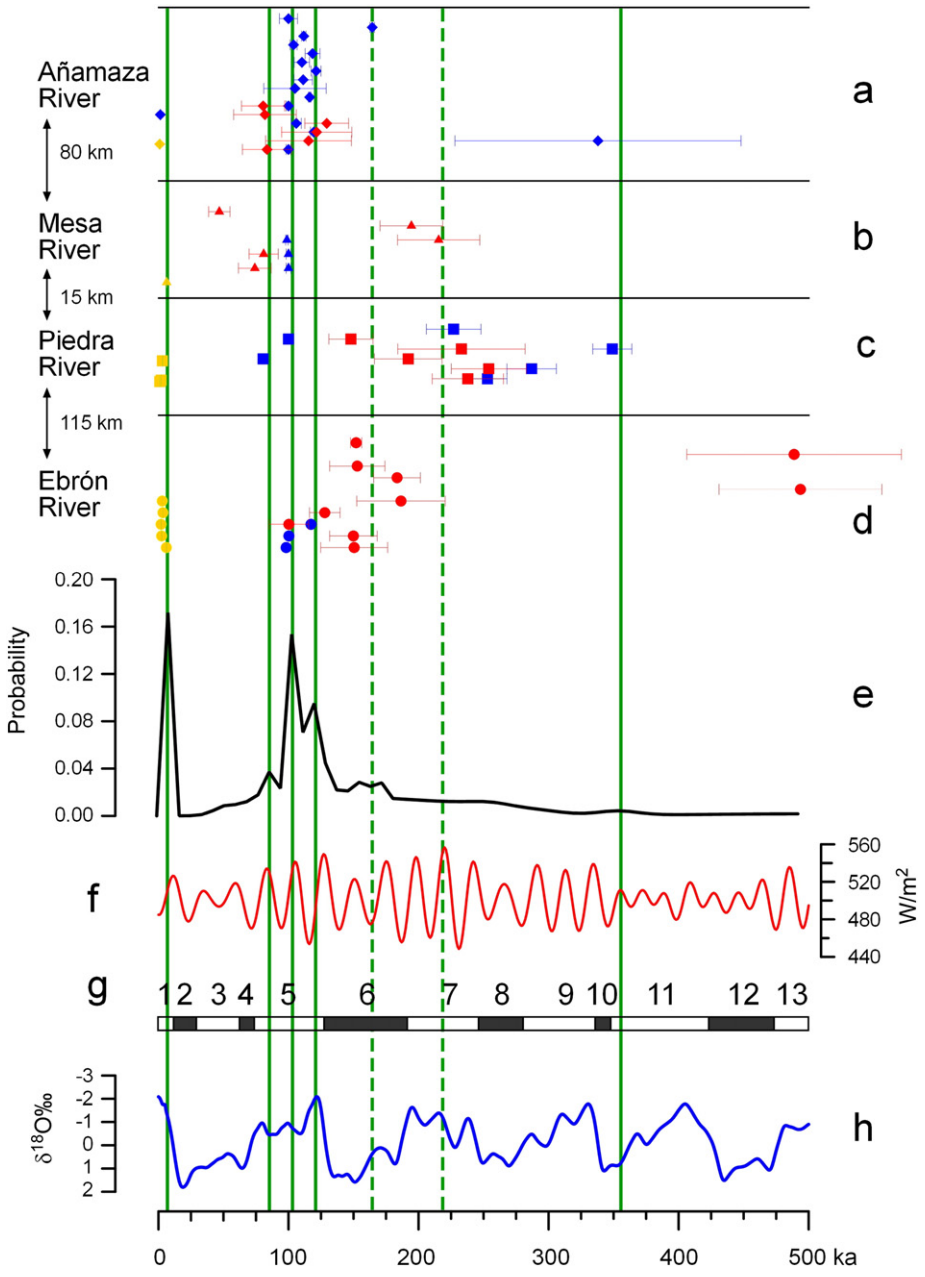

Fig. 9. Periods (vertical green lines) of active tufa deposition at 353 ka, 258–180 ka (centred dashed line), 171–154 ka (centred dashed line), 120 ka, 102 ka, 85 ka and 7 ka. Temporal distribution of tufa deposits in the Añamaza (diamonds) (a), Mesa (triangles) (b), Piedra (squares) (c) and Ebrón (circles) (d) valleys. Blue, red and yellow colour symbols refer to U/Th series, racemization and radiocarbon data, respectively. Cumulative probability density function plot of ages (e). Relationships to other palaeoenvironmental records: summer insolation at 42 °N (Berger and Loutre, 1991) (f), marine oxygen isotope stages (MIS) compilation (Bradley, 1999) (g) and SPECMAP isotope curve (Martinson et al., 1987) (h).

The Cascada stratigraphic section (E-2 section) (Figs. 4c and 8a) is 20 m thick. Four samples from the stratigraphic section (LC-4.4 y LC-B) and from a laterally equivalent deposit (LC-A y LC-B) were dated by AAR (Table 3). Samples from the section were corrected in the same way as sample MIR-5 above. Therefore, the age of this tufa build-up ranges between 150 and 98 ka. These ages were supported by U/Th data from a replicate sample (LC-3 A and B) that supplied ages of 117.3 and 117.4 ka (Table 2).

The thickness of the younger tufa unit exceeds 50 m. The Convento stratigraphic section (E-1 section) (Fig. 8a) (25 m thick) correspond to the upper part of this unit. The calibrated ^{14}C ages of three successive samples (CON-1, CON-7 and CON-9) are 6129–5982, 2489–2335 and 2065–1896 cal yr BP, respectively (Table 4), which are consistent with their stratigraphic position.

The Central (E-3 section) stratigraphic section (Fig. 8a), located approximately 1 km downstream of the El Convento section, is 25 m thick. The calibrated ages of 3475–3359 (sample CN-2) and 2961–2787 cal yr BP (CN-4) have been obtained by ^{14}C (Table 4). A comparison of ages by AAR (Table 3) and ^{14}C (Table 4) indicates that the AAR technique does not supply reliable and accurate ages for Holocene times, as the age calculation algorithms for the aspartic acid and glutamic acid D/L values were established for Pleistocene samples (Ortiz et al., 2004).

In summary, the distribution of the reliable ages obtained for the Ebrón River valley evidenced the occurrence of tufa deposition during MIS 6 and MIS 5 (180–100 ka) and MIS 1 (6–2 ka) (Figs. 8a and 9d). Evidence of older tufaceous deposits during MIS 13 (490 ka) should also be taken into consideration.

https://doi.org/10.1016/j.yqres.2015.08.003 Published online by Cambridge University Press

Discussion

Quaternary fluvial tufa deposits are widespread in the Añamaza, Mesa, Piedra and Ebrón rivers valleys, which are arranged N–S along 210 km in the Iberian Ranges (NE Spain). Several techniques were applied on tufa records to produce a reliable chronological approach that is well framed in both regional and global paleoclimatological contexts. A general agreement among the different techniques is observed, although U/Th dating provides ages of variable reliability according the features of the geochemistry of the tufa systems, and amino acid racemization does not yield accurate ages for Holocene tufa deposits. Nevertheless, the ages obtained through the several techniques can be considered consistent with the geomorphic position of build-ups and the location of samples in stratigraphic sections.

Chronological framework of tufa records and palaeoclimatic implications

Ages for the Quaternary Iberian Range tufa record derived from a multi-technique dating strategy provide a basis to decipher favourable conditions for tufa deposition and, therefore, to infer Quaternary palaeoclimatic implications in western Mediterranean areas.

The cumulative probability density function (CPDF), obtained from the summed individual probability distributions of the reliably dated tufa deposits (N = 64) (neither replicated ages nor AAR Holocene ages were considered), reveals several multi-millennial periods of tufa deposition in the studied sector of the Iberian Ranges (Fig. 9e). First, some tufa ages evidence an old period of tufa deposition during MIS 13 (ca. 490 ka) in the Ebrón River valley. Furthermore, the frequency distribution plot indicates that noticeable periods of tufa accumulation occurred at the end of MIS 11 (353 ka), the whole of MIS 7 (258–180 ka) and MIS 6 (171–154 ka). Nevertheless, the most active periods of tufa deposition coincide with MIS 5 (120 ka, 102 ka and 85 ka) and MIS 1 (7 ka) (Figs. 9g and h). It is remarkable that maximum frequency of tufa deposition during MIS 5 was identified at MIS 5e and mainly at MIS 5c substages, indicating more favourable palaeoenvironmental conditions during these short periods. MIS 3 is poorly represented, and the occurrence of MIS 3 tufas in this area remains uncertain. Correspondence between the increase in tufa development and interstadial MIS is widely recognized under temperate climates (Henning et al., 1983) and in the Iberian Peninsula (Domínguez-Villar et al., 2011; García-García et al., 2014; Martín-Algarra et al., 2003; Martínez-Tudela et al., 1986; Ordoñez et al., 2005; Ortiz et al., 2009). Some authors accentuate the relevance of humidity during interglacial periods in increasing tufa deposition rates in the Mediterranean region (Capezzuoli et al., 2010; Martínez-Tudela et al., 1986; Pedley, 2009). First data from speleothem growing stages in the NE Iberian Peninsula indicate that they are clearly connected to warm climates with positive hydrological balance and high insolation during interglacial periods (preferably MIS 7, MIS 5 and MIS 1) (Moreno et al., 2013). Moreover, the speleothem growth rate distribution in the NW Iberian Peninsula shows increasing intervals at ca. 200 MIS 7), 125, 105 and 85 ka (MIS 5e, MIS 5c and MIS 5a, respectively), and 9–6 ka (MIS 1). In the Iberian Ranges, the agreement between these speleothemic stages and the tufa deposition intervals is highly remarkable. However, more surprising is the extensive occurrence of tufa deposition during stadial stages. In fact, tufa formation, particularly during MIS 6, in the Iberian Ranges is not uncommon.

At a regional scale, the preferential accumulation of Quaternary tufa deposits during interglacial periods (Figs. 9g and h) in the Iberian Ranges broadly alternates with the occurrence of glacial and non-carbonate-bearing fluvial records in NE Spain (Pyrenees, Ebro Basin and Iberian Ranges) during cold phases (Fig. 9; vertical grey-shaded areas) (Benito et al., 2010; Fuller et al., 1998; García-Ruiz et al., 2013; Lewis et al., 2009; Sancho et al, 2008). Lewis et al. (2009), Benito et al. (2010) and García-Ruiz et al. (2013) recognize extensive fluvial terraces correlated to periods of glacial stability in glaciated headwaters of Pyrenean valleys (basins of the Aragón, Gállego and Cinca rivers) at 263, 178–140, 110–97, 68–61, 45–47, 17 and 11 ka. It has been established that the glacial system activity and the related fluvial dynamics seem sensitive to insolation controlled by orbital forcing (Lewis et al, 2009). In addition, Fuller et al. (1998) indicate that river aggradation episodes in the Guadalope River valley (Iberian Ranges) occurred at 183–130, 122, 111, 88, 49, 39–36, 24–22, 19–16, and 14–12 ka, and short Holocene stages. These alluviation phases were controlled by winter storm frequency under stadial periods with prevailing periglacial conditions.

However, this broad zipper-like environmental evolutionary model composed of alternative cold and warm long-term periods shows some inconsistencies. The occurrence of tufa deposits during the penultimate glaciation (MIS 6) in the Iberian Ranges is a quite different scenario from the other glacial periods. Consequently, the climate in this region, particularly during the onset of MIS 6 would not be as unfavourable as to preclude tufa formation. In the NE Iberian Peninsula, according to fluvial archives, the MIS 6 is characterized by high water availability in fluvial systems allowing the development of extensive fluvial terraces controlled by glacial outwash discharges and/or effective runoff (Benito et al., 2010) derived from increased seasonal storm frequency (Fuller et al., 1998). Moreover, at a regional scale, the penultimate glaciation (MIS 6) is characterized by an early phase comprising a sequence of warming-cooling events and a later phase with prolonged glacial conditions in the western Mediterranean (Martrat et al., 2004) and in the Portuguese margin (Margari et al., 2014). Stalagmite records from the northern Iberian Peninsula indicate periods of speleothem growth at 149–151 (Muñoz-García et al., 2007) and ca. 175 ka (Stoll et al., 2013), suggesting that carbonate precipitation persisted through the penultimate glaciation. In the same way, Wainer et al. (2013) suggest that MIS 6e was relatively warm and humid in south-western France from the speleothem record. Wilson et al. (2013) reported increased moisture availability during MIS 6.5 in Greece from lacustrine records. In brief, it seems likely that at lower latitudes, favourable conditions (warmer and wetter) during the early MIS 6 were enhanced because of the intensification of Asian and African monsoons (Wainer et al., 2013) and the related northward-deflected North Atlantic polar front (Calvo et al., 2001) within a context of maximal summer insolation (Stoll et al., 2013) and Earth's orbital variability (Margari et al., 2014).

Therefore, it seems that the tufa record in the Iberian Peninsula is sensitive to latitudinal shifts of atmospheric fronts and jet streams as well as perturbations in the North Atlantic, due to its location between high- and low-latitude regions. However, tufa deposition is not sensitive enough to the slight latitudinal and longitudinal gradient at the local scale. Tufa deposition in the four fluvial tufa systems located from N to S in the Iberian Ranges shows a similar temporal distribution. Thus, the tufa system response does not record significant changes in environmental conditions (source area and amount of rainfall and/or the vegetation cover) from more continental and Atlantic conditions in the Añamaza River valley (to the north) to more Mediterranean conditions in the Ebrón River valley (to the south).

Insolation is another environmental factor driving tufa accumulation that should be considered. In fact, the cumulative probability density function provides evidence for a close relationship between summer insolation peaks and tufa deposition episodes in the Iberian Ranges (Fig. 9f). Under humid climates, summer insolation would favour an increase in temperature, in soil CO_2 production and, consequently, in the CO_2 input in the karstic system dynamics. In endokarstic environments, Baldini et al. (2005) show a clear relationship between the speleothem growth rate and the degree of forest and shrub vegetation coverage. In fact, Stoll et al. (2013) indicate that hiatuses and reductions in stalagmite growth rate occur during extreme minima in summer insolation. Frank et al. (2000) also showed the influence of insolation on tufa formation is also apparent during the last interglaciation in the northern hemisphere (Southern Germany). The key role of insolation has also been shown from seasonal variations of tufa thickness in modern fluvial systems (e.g., Piedra River) (Arenas et al., 2014a).

https://doi.org/10.1016/j.yqres.2015.08.003 Published online by Cambridge University Press

Palaeoenvironmental setting

Climate during phases of tufa deposition in the Iberian Ranges was characterized by prevailing humid conditions producing high groundwater discharge. In addition to water availability, warm temperatures and insolation seem to reinforce the rates of tufa deposition. The resulting palaeoenvironmental context included the increase in forest vegetation cover, soil CO_2 production, exo- and endokarstic activity and the discharge of chemically active groundwater. This general biostatic context involves the biologically induced landscape stability (i.e., García del Cura et al., 1997; Goudie et al., 1993). Favourable conditions for tufa formation are intensified particularly during MIS 5, leading to the accumulation of the most important tufa deposits at a regional scale, which suggests wet and warm conditions over the last 500 ka in NE Iberia. Similar palaeoenvironmental conditions have also been interpreted at local, regional and continental scales (Dominguez-Villar et al., 2011; Frank et al., 2000; Henning et al., 1983; Ordoñez et al., 2005).

An increase of precipitation over the Mediterranean region under interstadial conditions has been deduced from the Alborán sea record (Moreno et al., 2002) and from growth rates of speleothem in the northern Iberian Peninsula (Stoll et al., 2013). In addition, a relationship between warm periods and increased global atmospheric CO_2 concentration has been observed from ice cores in Antarctica (Indermühle et al., 2000). The increase in atmospheric CO_2 favoured the increase in forest biomass (Higgins and Scheiter, 2012). Thus, higher temperature, precipitation and atmospheric CO_2 concentration favour the soil-vegetation productivity. Therefore, warm and humid conditions could favour a well-developed vegetation cover and a high production of soil CO_2. Under these conditions, solution processes were accelerated and, thus, ionic concentrations in groundwater discharges were increased.

In this environmental context, tufa deposition is triggered in the fluvial network when physical CO_2 outgassing is enhanced by the morphological discontinuities in the longitudinal profiles of the rivers. High gradient and stepped fluvial systems (sensu Arenas-Abad et al., 2010) showing different sedimentary architectures (barrage and dammed water areas, prograding–aggrading wedges and high gradient ramps with jumps) resulted in tufa build-ups in accordance with the local hydrological, geological and morphotopographic context.

In contrast, during phases of cold conditions (e.g., including wet MIS 4 and arid MIS 2, among others periods; Lewis et al., 2009), the deposition of tufa ceased, and fluvial incision partly destroyed the previous tufa deposits, developing a staircase terrace landscape. Erosion processes in fluvial tufa systems are strongly related to degradation of the vegetation cover on the slopes (Ordoñez et al., 2005) and to increased detrital supply from mechanical weathering. Actually, the resulting tufa build-ups sometimes include erosional episodes, when the previous tufa build-ups were partially destroyed. These episodes are most likely related to short stages of environmental deterioration with an increase of extreme hydrological events (Viles et al., 2007). These erosive events, related to extreme water discharge, are common in present-day fluvial tufa systems, controlling the development of tufa deposits (Vázquez-Urbez et al., 2010).

Conclusions

Enhanced chronology of the fluvial tufa record in a wide sector of the Iberian Ranges (NE Iberia), based on a multi-technique strategy, allow us to advance a proposal of a regional palaeoclimatic framework composed of sequential warm and wet stages during the last 500 ka. The following conclusions can be highlighted:

- The AAR, U/Th disequilibrium and radiocarbon ages produced consistent results, supported by geomorphic and stratigraphic field relations; although racemization appears inaccurate for Holocene samples.
- The regional tufaceous sequence includes periods of active tufa deposition at 353 (~MIS 11), 258–180 (MIS 7), 171–154 (MIS 6), 120 (MIS 5e), 102 (MIS 5c), 85 (~MIS 5a) and 7 ka (MIS 1). Major tufa growth stages occurred during MIS 5 and MIS 1, indicating warmer and wetter conditions than today.
- In addition to tufa deposition during interstadials, the occurrence of high tufaceous dynamics during MIS 6 is remarkable, as it indicates that the climate in the Iberian Peninsula was favourable to tufa deposition, mainly at the onset of the penultimate glacial stage.
- The tufa system behaviour in NE Iberia over the last 500 ka seems sensitive to summer solar forcing and to the precipitation regime in the western Mediterranean area, which is affected by latitudinal shifts of North Atlantic perturbations.

Acknowledgments

This research was supported by the Spanish Government and the European Regional Development Fund (projects CGL2006-05063/BTE, CGL2009-09216/CLI and CGL2009-10455/BTE). This is a contribution by Continental Sedimentary Basin Analysis and PaleoQ Groups (Aragón Government and University of Zaragoza). We would also like to thank Alan R. Gillespie (Editor), Peter Langdon (Associate Editor) and reviewers (B. Charlotte Schreiber and an anonymous person) for their valuable comments that helped to improve the manuscript. Thanks are also due to Prof. Lewis A. Owen for the final refinement of the manuscript.

References

Arenas, C., Sancho, C., Vázquez, M., Pardeo, G., Hellstrom, J., Ortiz, J.E., Torres, T., Osácar, C., Auqué, L., 2010. Las tobas cuaternarias del río Añamaza (provincia de Soria, Cordillera Ibérica): aproximación cronológica. Geogaceta 49, 51–54.

Arenas, C., Vázquez-Urbez, M., Auqué, L., Sancho, C., Osácar, M.C., Pardo, G., 2014a. Intrinsic and extrinsic controls of spatial and temporal variations in modern fluvial tufa sedimentation: a thirteen-year record from a semi-arid environment. Sedimentology 61, 90–132.

Arenas, C., Vázquez-Urbez, M., Pardo, G., Sancho, C., 2014b. Sedimentology and depositional architecture of tufas deposited in stepped fluvial systems of changing slope: lessons from the Quaternary Añamaza valley (Iberian Range, Spain). Sedimentology 61, 133–171.

Arenas, C., Auqué, L., Osácar, M.C., Sancho, C., Vázquez-Urbez, M., Pardo, G., 2015. Current tufa sedimentation in a high discharge river: a comparison with other synchronous tufa records in the Iberian Range (Spain). Sedimentary Geology 325, 132–157.

Arenas-Abad, C., Vázquez-Urbez, M., Pardo-Tirapu, G., Sancho-Marcén, C., 2010. Fluvial and associated carbonate deposits. In: Alonso-Zarza, A.M., Tanner, L.H. (Eds.), Carbonates in continental settings. Facies, environments and processesDevelopments in Sedimentology 61. Elsevier, Amsterdam, pp. 133–176.

Auqué, L., Arenas, C., Osácar, M.C., Pardo, G., Sancho, C., Vázquez-Urbez, M., 2013. Tufa sedimentation in changing hydrological conditions: the River Mesa (Spain). Geologica Acta 11, 85–102.

Auqué, L., Arenas, C., Osácar, C., Pardo, G., Sancho, C., Vázquez-Urbez, M., 2014. Current tufa sedimentation in a changing-slope valley: the River Añamaza (Iberian Range, NE Spain). Sedimentary Geology 303, 26–48.

Baker, A., Smart, P.L., Ford, D.C., 1993. Northwest European paleoclimate as indicated by growth frequency variations of secondary calcite deposits. Palaeogeography Palaeoclimatology Palaeoecology 100, 291–301.

Baldini, J.U.L., McDermott, F., Baker, A., Baldini, L.M., Mattey, D.P., Railsback, L.B., 2005. Biomass effects on stalagmite growth and isotope ratios: a 20th century analogue from Wiltshire, England. Earth and Planetary Science Letters 240, 486–494.

Benito, G., Sancho, C., Peña, J.L., Machado, M.J., Rhodes, E.J., 2010. Large-scale karst subsidence and accelerated fluvial aggradation during MIS6 in NE Spain: climatic and paleohydrological implications. Quaternary Science Reviews 29, 2694–2704.

Berger, A., Loutre, M.F., 1991. Insolation values for the climate of the last 10 million years. Quaternary Science Reviews 10, 297–317.

Bradley, R.S., 1999. Paleoclimatology. Academic Press, San Diego (613 pp.).

Brasier, A.T., 2011. Searching for travertines, calcretes and speleothems in deep time: processes, appearances, predictions and the impact of plants. Earth-Science Reviews 104, 213–239.

Bright, J., Kaufman, D.S., 2011. Amino acid racemization in lacustrine ostracodes, part I: effect of oxidizing pre-treatments on amino acid composition. Quaternary Geochronology 6, 154–173.

https://doi.org/10.1016/j.yqres.2015.08.003 Published online by Cambridge University Press

Cacho, I., Grimalt, J.O., Canals, M., 2002. Response of the Western Mediterranean Sea to rapid climatic variability during the last 50,000 years: a molecular biomarker approach. Journal of Marine Systems 33 (34), 253–272.
Calle, M., Sancho, C., Peña, J.L., Cunha, P., Oliva-Urcia, B., Pueyo, E., 2013. La secuencia de terrazas cuaternarias del río Alcanadre (provincia de Huesca): caracterización y consideraciones paleoambientales. Cuadernos de Investigación Geográfica 39, 159–178.
Calvo, E., Villanueva, J., Grimalt, J.O., Boelaert, A., Labeyrie, L., 2001. New insights into the glacial latitudinal temperature gradients in the North Atlantic. Results from $U^{K'}_{37}$ sea surface temperatures and terrigenous inputs. Earth and Planetary Science Letters 188, 509–519.
Capezzuoli, E., Gandin, A., Sandrelli, F., 2010. Calcareous tufa as indicators of climatic variability: a case study from southern Tuscany (Italy). Geological Society, London, Special Publications 336, 263–281.
Capezzuoli, E., Gandin, A., Pedley, H.M., 2014. Decoding tufa and travertine (freshwater carbonates) in the sedimentary record: the state of the art. Sedimentology 61, 1–21.
Cheng, H., Lawrence Edwards, R., Shen, C.-C., Polyak, V.J., Asmerom, Y., Woodhead, J.D., Hellstrom, J., Wang, Y., Kong, X., Spötl, C., Wang, X., Calvin Alexander Jr., E., 2013. Improvements in 230Th dating, 230Th and 234U half-life values, and U–Th isotopic measurements by multi-collector inductively coupled plasma mass spectrometry. Earth and Planetary Science Letters 371–372, 82–91.
Cremaschi, M., Zerboni, A., Spötl, Ch., Felletti, F., 2010. The calcareous tufa in the Tadrart Acacus Mt. (SW Fezzan, Libya). An early Holocene palaeoclimate archive in the central Shahara. Palaeogeography Palaeoclimatology Palaeoecology 287, 81–94.
Della Porta, G., 2015. Carbonate build-ups in lacustrine, hydrothermal and fluvial settings: comparing depositional geometry, fabric types and geochemical signature. In: Bosence, D.W.J., Gibbons, K.A., Le Heron, D.P., Morgan, W.A., Pritchard, T., Vining, B.A. (Eds.), Microbial Carbonates in Space and Time: Implications for Global Exploration and Production. Geological Society, London, Special Publications 418, pp. 17–68.
Domínguez-Villar, D., Vázquez-Navarro, J.A., Cheng, H., Edwards, R.L., 2011. Freshwater tufa record from Spain supports evidence for the past interglacial being wetter than the Holocene in the Mediterranean region. Global and Planetary Change 77, 129–141.
Durán, J.J., 1989. Geocronología de los depósitos asociados al karst en España. In: Durán, J.J., Martínez, J. (Eds.), El karst en España. Monografías Sociedad Española de Geomorfología 4, pp. 243–256.
Eynaud, F., Abreu, L., Voelker, A., Schönfeld, J., Salgueiro, E., Turon, J.L., Penaud, A., Toucanne, S., Naughton, F., Sánchez-Goñi, M.F., Malaizé, B., Cacho, I., 2009. Position of the Polar Front along the western Iberian margin during key cold episodes of the last 45 ka. Geochemistry, Geophysics, Geosystems 10, 1–21.
Ford, D., Pedley, H.M., 1996. A review of tufa and travertine deposits of the world. Earth-Science Reviews 41, 117–175.
Frank, N., Braum, M., Hambach, U., Mangini, A., Wagner, G., 2000. Warm period growth of travertine during the Last Interglaciation in southern Germany. Quaternary Research 54, 38–48.
Fuller, I.C., Macklin, M.G., Lewin, J., Passmore, D.G., Wintle, A.G., 1998. River response to high-frequency climate oscillations in southern Europe over the past 200 k.y. Geology 26, 275–278.
García del Cura, M.A., González-Martín, J.A., Ordóñez, S., Pedley, M., 1997. Las lagunas de Ruidera. In: García-Rayego, J.L., González-Cárdenas, E. (Eds.), Elementos del medio natural en la provincia de Ciudad RealColección Estudios 36. Ediciones de la Universidad de Castilla-La Mancha, pp. 85–129.
García-García, F., Pla-Pueyo, S., Nieto, L.M., Viseras, C., 2014. Sedimentology of geomorphologically controlled Quaternary tufas in a valley in southern Spain. Facies 60, 53–72.
García-Ruiz, J.M., Martí-Bono, C., Peña-Monné, J.L., Sancho, C., Rhodes, E.J., Valero-Garcés, B., González-Sampériz, P., Moreno, A., 2013. Glacial and fluvial deposits in the Aragón Valley, central-western Pyrenees: chronology of the Pyrenean late Pleistocene glaciers. Geografiska Annaler: Series A, Physical Geography 95, 15–32.
Goudie, A.S., Viles, H.A., Pentecost, A., 1993. The late-Holocene tufa decline in Europe. The Holocene 3, 181–186.
Gutiérrez, M., Peña, J.L., 1994. Cordillera Ibérica. In: Gutiérrez, M. (Ed.), Geomorfología de España. Editorial Rueda, pp. 251–286.
Gutiérrez, F., Gutiérrez, M., Gracia, F.J., McCalpin, J.P., Lucha, P., Guerrero, J., 2008. Plio-Quaternary extensional seismotectonics and drainage network development in the central sector of the Iberian Chain (NE Spain). Geomorphology 102, 21–42.
Hearty, P.J., O'Leary, M.J., Kaufman, D.S., Page, M.C., Bright, J., 2004. Amino acid geochronology of individual foraminifer (*Pulleniatina obliquiloculata*) tests, north Queenland margin, Australia: a new approach to correlating and dating Quaternary tropical marine sediment cores. Paleoceanography 19, PA4022. http://dx.doi.org/10.1029/2004PA001059.
Hellstrom, J., 2003. Rapid and accurate U/Th dating using parallel ion-counting multi-collector ICP-MS. Journal of Analytical Atomic Spectrometry 18, 1346–1351.
Hellstrom, J., 2006. U–Th dating of speleothems with high initial 230Th using stratigraphical constraint. Quaternary Geochronology 1, 289–295.
Henning, G.J., Grun, R., Brunnacker, K., 1983. Speleothems, travertins and paleoclimates. Quaternary Research 20, 1–29.
Higgins, S.I., Scheiter, S., 2012. Atmospheric CO_2 forces abrupt vegetation shifts locally, but not globally. Nature 488, 209–212.
Indermühle, A., Monnin, E., Stauffer, B., Stocker, T.F., Wahlen, M., 2000. Atmospheric CO_2 concentration from 60 to 20 kyr BP from the Taylor Dome ice core, Antarctica. Geophysical Research Letters 27, 735–738.
Kaufman, D.S., 2000. Amino acid racemization in ostracodes. In: Goodfriend, G.A., Collins, M.J., Fogel, M.L., Macko, S.A., Wehmiller, J.F. (Eds.), Perspectives in Amino Acids and Protein Geochemistry. Oxford University Press, New York, pp. 145–160.
Kaufman, D.S., 2006. Temperature sensitivity of aspartic and glutamic acid racemization in the foraminifera Pulleniatina. Quaternary Geochronology 1, 188–207.
Kaufman, D.S., Manley, W.F., 1998. A new procedure for determining DL amino acid ratios in fossils using reverse phase liquid chromatography. Quaternary Geochronology 17, 987–1000.
Kronfeld, J., Vogel, J.C., Rosenthal, E., Weinstein-Evron, M., 1988. Age and paleoclimatic implications of the Bet Shean travertines. Quaternary Research 30, 298–303.
Lewis, C., McDonald, E., Sancho, C., Peña, J.L., Rhodes, E., 2009. Climatic implications of correlated Upper Pleistocene glacial and fluvial deposits on the Cinca and Gállego Rivers (NE Spain) based on OSL dating and soil stratigraphy. Global and Planetary Change 67, 141–152.
Livnat, A., Kronfeld, J., 1985. Paleoclimatic implications of U-series dates for lake sediments and travertines in the Arava Rift Valley, Israel. Quaternary Research 24, 164–172.
Lozano, M.V., Sancho, C., Arenas, C., Vázquez-Urbez, M., Ortiz, J.E., Torres, T., Pardo, G., Osácar, M.C., Auqué, L., 2012. Análisis preliminar de las tobas cuaternarias del río Ebrón (Castielfabib, Valencia, Cordillera Ibérica). Geogaceta 51, 55–58.
Luzón, M.A., Pérez, A., Borrego, A.G., Mayayo, M.J., Soria, A.R., 2011. Interrelated continental sedimentary environments in the central Iberian Range (Spain): Facies characterization and main palaeoenvironmental changes during the Holocene. Sedimentary Geology 239, 87–103.
Magnin, F., Guendon, J.L., Vaudour, J., Martin, Ph., 1991. Les travertins: accumulations carbonatées associées aux systèmes karstiques, séquences sédimentaires et paléoenvironnements quaternaires. Bulletin de la Societe Geologique de France 162, 585–594.
Margari, V., Skinner, L.C., Hodell, D.A., Martrat, B., Toucanne, S., Grimalt, J.O., Gibbard, P.L., Lunkka, J.P., Tzedakis, P.C., 2014. Land–ocean changes on orbital and millennial time scales and the penultimate glaciation. Geology 42, 183–186.
Martín-Algarra, A., Martín-Marín, M., Andreo, B., Julià, R., González-Gómez, C., 2003. Sedimentary patterns in perched spring travertines near Granada (Spain) as indicators of the paleohydrological and paleoclimatological evolution of a karst massif. Sedimentary Geology 161, 217–228.
Martínez-Tudela, A., Cuenca, F., Santisteban, C., Grun, R., Hentzsch, B., 1986. Los travertinos del Río Matarraña, Beceite (Teruel) como indicadores paleoclimáticos del Cuaternario. In: López-Vera, F. (Ed.), Quaternary Climate in Western Mediterranean. Universidad Autónoma de Madrid, pp. 307–324.
Martinson, D.G., Pisias, N., Hays, J.D., Imbrie, J., Moore, T.C., Shackleton, N.J., 1987. Age dating and the orbital theory of the Ice Ages: development of a high resolution 0 to 300,000-year chronostratigraphy. Quaternary Research 27, 1–29.
Martrat, B., Grimalt, J.O., Lopez-Martinez, C., Cacho, I., Sierro, F.J., Flores, J.A., Zahn, R., Canals, M., Curtis, J.H., Hodell, D.A., 2004. Abrupt temperature changes in the western Mediterranean over the past 250,000 years. Science 306, 1762–1765.
Moreno, A., Cacho, I., Canals, M., Prins, M.A., Sánchez Goñi, M.F., Grimalt, J.O., Weltje, G.J., 2002. Saharan dust transport and high-latitude glacial climatic variability: the Alboran Sea record. Quaternary Research 58, 318–328.
Moreno, A., Cacho, I., Canals, M., Grimalt, J.O., Sánchez Goñi, M.F., Shackleton, N., Sierro, F.J., 2005. Links between marine and atmospheric processes oscillating on a millennial time-scale. A multi-proxy study of the last 50,000 yr from the Alboran Sea (Western Mediterranean Sea). Quaternary Science Reviews 24, 1623–1636.
Moreno, A., Belmonte, A., Bartolomé, M., Sancho, C., Oliva, B., Stoll, H., Edwards, L.R., Cheng, H., Hellstrom, J., 2013. Formación de espeleotemas en el noreste peninsular y su relación con las condiciones climáticas durante los últimos ciclos glaciares. Cuadernos de Investigación Geográfica 39, 27–47.
Muñoz-García, M.B., Martín-Chivelet, J., Rossi, C., Ford, D.C., Schwarcz, H.P., 2007. Chronology of Termination II and the Last Interglacial Period in North Spain based on stable isotope records of stalagmites from Cueva del Cobre (Palencia). Journal of Iberian Geology 33, 17–30.
Ordoñez, S., González Martín, J.A., García del Cura, M.A., Pedley, H.M., 2005. Temperate and semi-arid tufas in the Pleistocene to Recent fluvial barrage system in the Mediterranean area: the Ruidera Lakes Natural Park (Central Spain). Geomorphology 69, 332–350.
Ortiz, J.E., Torres, T., Julià, R., Delgado, A., Llamas, F.J., Soler, V., Delgado, J., 2004. Numerical dating algorithms of amino acid racemization ratios from continental ostracodes. Application to Guadix-Baza basin (southern Spain). Quaternary Science Reviews 23, 717–730.
Ortiz, J.E., Torres, T., Delgado, A., Reyes, E., Díaz-Bautista, A., 2009. A review of the Tagus river tufa deposits (central Spain): age and palaeoenvironmental record. Quaternary Science Reviews 28, 947–963.
Ortiz, J.E., Torres, T., Pérez-González, A., 2013. Amino acid racemization in four species of ostracodes: taxonomic, environmental, and microstructural controls. Quaternary Geochronology 16, 129–143.
Osácar, M.C., Arenas, C., Vázquez-Urbez, M., Sancho, C., Auqué, L., Pardo, G., Lojen, S., Cukrov, N., 2013. Seasonal and decadal stable isotope evolution recorded by recent tufa deposited on artificial substrates in the Monasterio de Piedra Natural Park (NE Spain). Geogaceta 54, 135–138.
Pazdur, A., Pazdur, M.F., Starkel, L., Szulc, J., 1988. Stable isotopes of Holocene calcareous tufa in southern Poland as palaeoclimatic indicators. Quaternary Research 30, 177–189.
Pedley, H.M., 1990. Classification and environmental models of cool freshwater tufas. Sedimentary Geology 68, 143–154.
Pedley, H.M., 1993. Sedimentology of the late Quaternary barrage tufas in the Wye and Lathkill valleys, north Derbyshire. Proceedings of the Yorkshire Geological Society 49, 197–206.
Pedley, M., 2009. Tufas and travertines of the Mediterranean region: a testing ground for freshwater carbonate concepts and developments. Sedimentology 56, 221–246.
Pedley, M., Andrews, J., Ordoñez, S., García del Cura, M.A., González Martín, J.A., Taylor, D., 1996. Does climate control the morphological fabric of freshwater carbonates?

https://doi.org/10.1016/j.yqres.2015.08.003 Published online by Cambridge University Press

A comparative study of Holocene barrage tufas from Spain and Britain. Palaeogeography Palaeoclimatology Palaeoecology 121, 239–257.
Peña, J.L., Gutiérrez, M., Ibáñez, M.J., Lozano, M.V., Rodríguez, J., Sánchez, M., Simón, J.L., Soriano, A., Yetano, L.M., 1984. Geomorfología de la Provincia de Teruel. Instituto de Estudios Turolenses (149 pp.).
Pentecost, A., 1995. The Quaternary travertine deposits of Europe and Asia Minor. Quaternary Science Reviews 14, 1005–1028.
Pérez-Sanz, A., González-Sampériz, P., Moreno, A., Valero-Garcés, B., Gil-Romera, G., Rieradevall, M., Tarrats, P., Lasheras-Álvarez, L., Morellón, M., Belmonte, A., Sancho, C., Sevilla-Callejo, M., Navas, A., 2013. Holocene climate variability, vegetation dynamics and fire regime in the central Pyrenees: the Basa de la Mora sequence (NE Spain). Quaternary Science Reviews 73, 149–169.
Reimer, P.J., Baillie, M.G.L., Bard, E., Bayliss, A., Beck, J.W., Blackwell, P.G., Bronk Ramsey, C., Buck, C.E., Burr, G.S., Edwards, R.L., Friedrich, M., Grootes, P.M., Guilderson, T.P., Hajdas, I., Heaton, T.J., Hogg, A.G., Hughen, K.A., Kaiser, K.F., Kromer, B., McCormac, F.G., Manning, S.W., Reimer, R.W., Richards, D.A., Southon, J.R., Talamo, S., Turney, C.S.M., van der Plicht, J., Weyhenmeyer, C.E., 2009. IntCal09 and Marine09 radiocarbon age calibration curves, 0–50,000 years cal BP. Radiocarbon 5, 1111–1150.
Sancho, C., Muñoz, A., Rhodes, E., McDonald, E., Peña, J.L., Benito, G., Longares, L.A., 2008. Morfoestratigrafía y cronología de registros fluviales del Pleistoceno superior en Bardenas Reales de Navarra: implicaciones paleoambientales. Geogaceta 45, 47–50.
Sancho, C., Arenas, C., Pardo, G., Vázquez, M., Hellstrom, J., Ortiz, J.E., Torres, T., Rhodes, E., Osácar, C., Auqué, L., 2010. Ensayo cronológico de las tobas cuaternarias del río Piedra (Cordillera Ibérica). Geogaceta 48, 31–34.
Scotti, V.N., Molina, P., Faccenna, C., Soligo, M., Casas-Sainz, A., 2014. The influence of surface and tectonic processes on landscape evolution of the Iberian Chain (Spain): quantitative geomorphological analysis and geochronology. Geomorphology 206, 37–57.
Smith, J.R., Giegengack, R., Schwarcz, H.P., 2004. Constraints on Pleistocene pluvial climates through stable-isotope analysis of fossil-spring tufas and associated gastropods, Kharga Oasis, Egypt. Palaeogeography Palaeoclimatology Palaeoecology 206, 157–175.
Stoll, H.M., Moreno, A., Mendez-Vicente, A., Gonzalez-Lemos, S., Jimenez-Sanchez, M., Dominguez-Cuesta, M.J., Edwards, R.L., Cheng, H., Wang, X., 2013. Paleoclimate and growth rates of speleothems in the northwestern Iberian Peninsula over the last two glacial cycles. Quaternary Research 80, 284–290.
Stuiver, M., Reimer, P.J., 1993. Extended ^{14}C database and revised CALIB radiocarbon calibration program. Radiocarbon 3, 215–230.
Vázquez-Urbez, M., Arenas, C., Sancho, C., Osácar, M.C., Auqué, L., Pardo, G., 2010. Factors controlling present-day tufa dynamics in the Monasterio de Piedra Natural Park (Iberian Range, Spain): depositional environmental settings, sedimentation rates and hydrochemistry. International Journal of Earth Sciences 99, 1027–1049.
Vázquez-Urbez, M., Pardo, G., Arenas, C., Sancho, C., 2011a. Fluvial diffluence episodes reflected in the Pleistocene tufa deposits of the River Piedra (Iberian Range, NE Spain). Geomorphology 125, 1–10.
Vázquez-Urbez, M., Arenas, C., Sancho, C., Auqué, L., Osácar, C., Pardo, G., 2011b. Quaternary and present-day tufa Systems of the Rivers Piedra and Añamaza (Iberian Range, Spain). In: Arenas, C., Pomar, L., Colombo, F. (Eds.), Field trips 28th IAS Meeting, ZaragozaGeo-Guías 8. International Association of Sedimentologists-Sociedad Geológica de España, pp. 241–274.
Vázquez-Urbez, M., Arenas, C., Pardo, G., 2012. A sedimentary facies model for stepped, fluvial tufa systems in the Iberian Range (Spain): the Quaternary Piedra and Mesa valleys. Sedimentology 59, 502–526.
Viles, H.A., Goudie, A.S., 1990. Tufas, travertines and allied carbonate deposits. Progress in Physical Geography 14, 19–41.
Viles, H.A., Taylor, M.P., Nicoll, K., Neumann, S., 2007. Facies evidence of hydroclimatic regime shifts in tufa depositional sequences from the arid Naukluft Mountains, Namibia. Sedimentary Geology 195, 39–53.
Wainer, K., Genty, D., Blamart, D., Bar-Matthews, M., Quinif, Y., Plagnes, V., 2013. Millennial climatic instability during penuntimate glacial periods recorded in a south-western France speleothem. Palaeogeography Palaeoclimatology Palaeoecology 376, 122–131.
Wilson, G.P., Frogley, M.R., Roucoux, K.H., Jones, T.D., Leng, M.J., Lawson, I.T., Hughes, P.D., 2013. Limnetic and terrestrial responses to climate change during the onset of the penultimate glacial stage in NW Greece. Global and Planetary Change 107, 213–225.

https://doi.org/10.1016/j.yqres.2015.08.003 Published online by Cambridge University Press